Geophys. J. Int. (2004) **157,** 455–473 doi: 10.1111/j.1365-246X.2004.02198.x

Standing torsional waves in a fully saturated, porous, circular cylinder

Selene Solorza and Pratap N. Sahay*

Department of Seismology, Centro de Investigación Científica y de Educación Superior de Ensenada, Ensenada, Baja California 22860, *Mexico.*

Accepted 2003 November 11. Received 2003 October 10; in original form 2003 January 6

SUMMARY

For dynamic measurement of the elastic moduli of a porous material saturated with viscous fluid using the resonance-bar technique, one also observes attenuation. In this article we have carried out the solution of the boundary-value problem associated with standing torsional oscillations of a finite, poroelastic, circular cylinder cast in the framework of volume-averaged theory of poroelasticity. Analysing this solution by eigenvalue perturbation approach we are able to develop expressions for torsional resonance and temporal attenuation frequencies in which the dependence upon the material properties are transparent. It shows how the attenuation is controlled by the permeability and the fluid properties, and how the resonance frequency drops over its value for the dry solid-frame due to the drag effect of fluid mass. Based upon this work we have a firm basis to determine solid-frame shear modulus, permeability, and tortuosity factor from torsional oscillation experiments.

Key words: porous media, standing waves, torsional waves.

1 INTRODUCTION

The resonance-bar technique is often used to determine the elastic moduli of a solid. In this method a solid core of cylindrical or rectangular cross-section of finite length is excited into a characteristic mode of a standing wave, such as torsional, longitudinal or flexural, and the resonance frequency is recorded. The resonance frequency for the case of the torsional mode of vibration is linked to rigidity. For the longitudinal mode it is related to Young's modulus and Poisson's ratio, and for the flexural mode it is linked to Young's modulus.

When this method is applied to a poroelastic sample (i.e. a solid matrix saturated with viscous fluid), one also observes attenuation of the wavefield. Currently it is interpreted in terms of solid viscosity by assuming a viscoelastic rheology for the porous material (O'Hara 1985; Bourbie *et al.* 1987; Sothcott *et al.* 2000). The motion of the fluid with respect to the solid-frame and the viscous loss within the pore fluid are the two likely mechanisms of attenuation in a fluid-saturated, porous material. So it is appropriate to assume a poroelastic rheology and work out the appropriate boundary-value problem to link the observed resonance frequency and attenuation values with the properties of the solid and fluid constituents and permeability. In this article we have worked out such a formula for the case of torsional oscillation of a finite, fully-saturated, homogeneous and isotropic porous cylinder.

The theory of wave propagation in porous media was introduced in the middle of the last century by Biot (1956, 1962). Recently, by volume averaging pore-scale dynamic equations, a theory of poroelasticity has been develop on a firm basis (de la Cruz & Spanos 1985, 1989; de la Cruz *et al.* 1993; Hickey *et al.* 1995; Sahay 1996; Sahay *et al.* 2001), wherein change in porosity during deformation is explicitly present in the constitutive relations. The Biot theory is shown to be a limiting case of this framework: in it the change in porosity during deformation is only affected by the difference in pressures of the two phases only (Sahay 2001). Furthermore, the only loss mechanism in the Biot theory is the motion of the fluid with respect to the solid frame, i.e. the Darcian dissipation term. The viscous loss within the pore fluid is not included in the Biot theory. The volume-averaged constitutive relations incorporates the internal viscous loss process as a relaxation term in a natural way, in addition to the usual Darcian dissipation process. It should be noted that this relaxation process gives a wavenumber dependent loss, whereas the Darcian dissipation loss is independent of wavenumber. For a porous sample saturated with highly viscous fluid, such as heavy crude oil or bitumen, this relaxation process is of importance. Although, for a homogeneous and isotropic case, change in porosity during deformation affects only a compressional deformation process and thus is not a part of the torsional deformation process under consideration,

*Correspondence address: Department of Seismology, CICESE, PO Box 434843, San Diego CA 92143, USA.

in order to properly take into account pore-fluid viscous relaxation, we will carry out this study in the framework of the volume-averaged theory of poroelasticity. Dunn (1986) has carried out a formal solution of this problem but has done so in the framework of the Biot theory, also, he does not give an explicit formula linking the resonance frequency and attenuation to the material properties and permeability.

In Section 2 the standing-torsional-wave problem, in the framework of volume-averaged theory of poroelasticity, is formulated as a 2 × 2 matrix wave equation with dissipation and relaxation terms. In the following section, the general solution is obtained using an eigenfunction approach. The expressions for the torsional resonance and temporal attenuation frequencies thus obtained are algebraically complicated to show the material properties dependence in a transparent manner. In Section 4 these expressions are reworked by eigenvalue perturbation approach such that the link with material properties are transparent. The approach seeks a transformation of the displacement field vector, and views the diagonal part of the transformed wave operator as the unperturbed (or zeroth-order) operator and the off-diagonal part of the transformed wave operator as the perturbation. The transformation is chosen such that the resonance and temporal attenuation frequencies given by the unperturbed operator are close to the exact values. The unperturbed operator, being diagonal, renders the expressions for (zeroth-order) resonance and temporal attenuation frequencies in a straightforward manner. This analysis shows how the attenuation is controlled by permeability and the fluid's shear viscosity, and how the resonance frequency drops compared to its dry-frame value due to the effect of fluid mass. Finally, we discuss the implications of our results and present concluding remarks in Section 5.

2 STATEMENT OF THE PROBLEM

Let a poroelastic circular cylinder of radius a and length H undergo an angular displacement independent of the angle such that there are no axial or radial displacements. This means that the cross-section of the cylinder rotates without distortion. The volume-averaged equations of motion of poroelasticity (Sahay 1996) for the angular displacement field, **u**, expressed in cylindrical coordinates are

$$\left(\mathbf{C}+\mathbf{N}\frac{\partial}{\partial t}\right)\left[\frac{1}{r}\frac{\partial}{\partial r}\left(r\frac{\partial}{\partial r}\right)+\frac{\partial^2}{\partial z^2}-\frac{1}{r^2}\right]\mathbf{u}=\Omega_{\mathrm{i}}\mathbf{I}_0\frac{\partial \mathbf{u}}{\partial t}+\mathbf{I}\frac{\partial^2\mathbf{u}}{\partial t^2}. \tag{1}$$

The **u** is a two-component vector $(u^{\mathrm{m}}, u^{\mathrm{i}})^{\mathrm{T}}$ ($^{\mathrm{T}}$ stands for transpose). u^{m} is the sum of mass-weighted angular displacements of the solid and fluid phases (centre-of-mass field). u^{i} is the difference of the angular displacements (internal field) of two phases. Although a dynamic problem can also be studies in terms of phasic field variables, namely solid and fluid displacement fields, it is shown in Sahay (1996) that centre-of-mass and internal fields are the natural dynamic field variables. These two frameworks are interconnected by a linear transformation which is stated in eq. (A9). The centre-of-mass field is associated with total linear-momentum flux, whereas the internal field is associated with the relative acceleration of two phases and it describes spin (angular momentum about the mass centre) flux. Since geophones register the field associated with total linear-momentum, they in fact track the centre-of-mass field. The internal field amounts to fluid flow because it is the motion of fluid relative to the solid-frame. While the internal field is not detected directly, its effect is measured via the attenuation of the centre-of-mass field.

The elements of the second-order **C** matrix have dimensions of velocity squared and they contain the frame shear modulus and frame and fluid densities. The elements of the second-order **N** matrix have dimensions of kinematic viscosity and they contain the fluid shear viscosity. This matrix accounts for viscous loss within the pore fluid. Ω_{i} is the relaxation frequency corresponding to the dissipation due to fluid flow with respect to the solid-frame and it contains a permeability term. In fact, it is akin to the well known Biot critical frequency. The second-order matrix $\mathbf{I}_0$ associated with Ω_{i} has all of its elements, except one, equal to zero. **I** is the 2 × 2 identity matrix associated with the inertial terms. The explicit expressions of these parameters are given in Appendix A.

For the problem under consideration, first we determine the complete set of eigenfunctions and associated eigenvalues for eq. (1) for the case of a finite cylinder with the stress-free surface: namely, the radial surface ($r = a$) and the top ($z = \mathrm{H}$) and bottom ($z = 0$) end-caps. The stress-free boundary conditions are taken from Sahay (1996), see Section 5:

$$\sigma^{\mathrm{m}}_{r\theta}\big|_{r=a}=0,\ \sigma^{\mathrm{i}}_{r\theta}\big|_{r=a}=0,\ \sigma^{\mathrm{m}}_{\theta z}\big|_{z=0}=0,\ \sigma^{\mathrm{i}}_{\theta z}\big|_{z=0}=0,\ \sigma^{\mathrm{m}}_{\theta z}\big|_{z=\mathrm{H}}=0,\ \sigma^{\mathrm{i}}_{\theta z}\big|_{z=\mathrm{H}}=0. \tag{2}$$

The explicit expressions for σ^{m}_{jk}, the total stress of the porous medium, and σ^{i}_{jk}, the stress associated with the relative acceleration of two phases, are given in Appendix B. Subsequently, nearly equal to these exact eigenvalues, we construct approximate eigenvalues by utilizing eigenvalue perturbation approach. This leads to the expressions for resonance and attenuation frequencies, wherein dependence on material properties are explicitly apparent.

3 GENERAL SOLUTION OF THE PROBLEM

3.1 Eigenfunction expansion

We expand the solution in terms of appropriate orthonormal basis functions in radial and axial coordinates that automatically satisfy the boundary conditions eq. (2). These choices reduce the equations of motion eq. (1) to a system of two coupled, second-order ordinary differential equations (in time). The solution is then obtained in a straight forward manner.

Because of the cylindrical geometry of the problem, one may take the Bessel function of first-order, $J_1(kr)$, and the cosine function, $\cos(lz)$, as the appropriate basis functions to express the spatial part of displacement fields governed by the differential eq. (1). To satisfy the

boundary conditions on the radial surface (eq. 2 in conjunction with eqs B1 and B2) one requires that $r\frac{\partial}{\partial r}(\frac{J_1(kr)}{r})|_{r=a} = 0$, which restricts the radial wavenumber k to be a discrete set defined as $k_p = \frac{N_p}{a}$, where N_p is the pth root of the Bessel function of second-order. These Bessel functions form an orthonormal complete set over the interval $0 \leq r \leq a$. In order to satisfy the boundary conditions on the end-caps (eq. 2 in conjunction with eqs B3 and B4) one requires that the $\frac{\partial}{\partial z}$ derivative of the axial function $\cos(lz)$ vanishes at $z = 0$ and $z = \mathrm{H}$: these conditions restrict the axial wavenumber l to be a discrete set given as $l_q = \frac{q\pi}{\mathrm{H}}$, where q is an integer. These cosine functions form an orthonormal complete set over the interval $0 \leq z \leq \mathrm{H}$. Hence, we take the solution to be of the form

$$\mathbf{u}(r, z, t) = \sum_{p=1}^{\infty}\sum_{q=1}^{\infty} k_p J_1(k_p r)\cos(l_q z)\mathbf{U}(t; k_p, l_q), \tag{3}$$

which satisfies the boundary conditions eq. (2). Then eq. (1) yields the temporal part of displacement field vector, $\mathbf{U} = (\mathrm{U^m}, \mathrm{U^i})^{\mathrm{T}}$, which is governed by a system of two coupled damped harmonic oscillators

$$\left[\mathbf{I}\frac{d^2}{dt^2} + (\Omega_{\mathrm{i}}\mathbf{I}_0 + \boldsymbol{\nu})\frac{d}{dt} + \mathbf{W}\right]\mathbf{U} = 0 \text{ or in a compact notation } \left(\mathbf{I}\frac{d^2}{dt^2} + \boldsymbol{\mathcal{D}}\right)\mathbf{U} = 0, \tag{4}$$

where

$$\mathbf{W} = \left(k_p^2 + l_q^2\right)\mathbf{C}, \tag{5}$$

$$\boldsymbol{\nu} = \left(k_p^2 + l_q^2\right)\mathbf{N}, \tag{6}$$

$$\boldsymbol{\mathcal{D}} \equiv (\Omega_{\mathrm{i}}\mathbf{I}_0 + \boldsymbol{\nu})\frac{d}{dt} + \mathbf{W}. \tag{7}$$

The matrix $\mathbf{W}$, which is the matrix $\mathbf{C}$ weighted by the square of the wavenumber, has dimensions of frequency squared. As it is associated with the elastic stiffness, it may be regarded as the fundamental-frequency (squared) matrix of the system. The matrix $\boldsymbol{\nu}$, which is the kinematic viscosity matrix $\mathbf{N}$ weighted by the square of the wavenumber, also has dimensions of frequency. Thus, it is the wavenumber-dependent damping matrix due to viscous loss within the pore fluid. The explicit expressions of these matrices are given in Appendix A.

3.2 Eigenfrequency

We seek a solution of eq. (4) of the form $e^{-i\omega(k_p, l_q)t}$ and obtain the 4th-order characteristic polynomial

$$\begin{aligned}\omega\left\{\omega^3 + i[\Omega_{\mathrm{i}} + Tr(\boldsymbol{\nu})]\omega^2 \right. &- [Tr(\mathbf{W}) + \Omega_{\mathrm{i}}\upsilon^{\mathrm{mm}}]\,\omega \\ &\left. - \, i\,[\Omega_{\mathrm{i}}W^{\mathrm{mm}} + Tr(\mathbf{W})Tr(\boldsymbol{\nu}) - Tr(\mathbf{W}\boldsymbol{\nu})]\right\} = 0.\end{aligned} \tag{8}$$

Hereafter, $Tr()$ stands for the trace of the matrix within the braces. $\omega = 0$ is the trivial root of eq. (8) (hereafter it is labelled as ω_4). The remaining three discrete (complex) frequencies associated with torsional-eigenvibrations are determined by solving the cubic polynomial within the curly braces in eq. (8). Utilizing the CRC standard mathematical tables (Selby 1971, p. 103) we find the roots to be

$$\omega_1(k_p, l_q) = -\frac{A+B}{2} + i\left(\sqrt{3}\frac{A-B}{2} - \frac{h}{3}\right),$$

$$\omega_2(k_p, l_q) = A + B - i\frac{h}{3},$$

$$\omega_3(k_p, l_q) = -\frac{A+B}{2} - i\left(\sqrt{3}\frac{A-B}{2} + \frac{h}{3}\right)$$

where

$$A = i^{(1/3)}\left(-\frac{d}{2} + \sqrt{\frac{d^2}{4} - \frac{b^3}{27}}\right)^{(1/3)},$$

$$B = -i^{(1/3)}\left(\frac{d}{2} + \sqrt{\frac{d^2}{4} - \frac{b^3}{27}}\right)^{(1/3)},$$

$$b = \frac{1}{3}(3f + h^2),$$

$$d = \frac{1}{27}(27g - 2h^3 - 9hf),$$

$$h = \Omega_{\mathrm{i}} + Tr(\boldsymbol{\nu}),$$

$$f = -\left[Tr\left(\mathbf{W}\right) + \Omega_{\mathrm{i}}\upsilon^{\mathrm{mm}}\right],$$

$$g = -\left[\Omega_{\mathrm{i}}W^{\mathrm{mm}} + Tr(\mathbf{W})Tr(\boldsymbol{\nu}) - Tr(\mathbf{W}\boldsymbol{\nu})\right].$$

Given that $B = -\frac{1}{3}\frac{b}{A}$ and $A_{\rm R} = \sqrt{3}A_{\rm I}$, where $A_{\rm R}$ and $A_{\rm I}$ are the real and imaginary parts of A, respectively, the three complex roots are found to be

$$\omega_1(k_p, l_q) = A_{\rm R}\frac{b - 3\left(A_{\rm R}^2 + A_{\rm I}^2\right)}{3\left(A_{\rm R}^2 + A_{\rm I}^2\right)} - \frac{i}{3}\left[h - A_{\rm I}\frac{b + 3\left(A_{\rm R}^2 + A_{\rm I}^2\right)}{\left(A_{\rm R}^2 + A_{\rm I}^2\right)}\right], \tag{9}$$

$$\omega_2(k_p, l_q) = -A_{\rm R}\frac{b - 3\left(A_{\rm R}^2 + A_{\rm I}^2\right)}{3\left(A_{\rm R}^2 + A_{\rm I}^2\right)} - \frac{i}{3}\left[h - A_{\rm I}\frac{b + 3\left(A_{\rm R}^2 + A_{\rm I}^2\right)}{3\left(A_{\rm R}^2 + A_{\rm I}^2\right)}\right], \tag{10}$$

$$\omega_3(k_p, l_q) = -\frac{i}{3}\left[h + 2A_{\rm I}\frac{b + 3\left(A_{\rm R}^2 + A_{\rm I}^2\right)}{\left(A_{\rm R}^2 + A_{\rm I}^2\right)}\right]. \tag{11}$$

For realistic parameters for geomaterials, the quantity $\frac{d^2}{4} - \frac{b^3}{27} > 0$ and $d < 0$, which implies the real and imaginary parts of A are positive and $h > A_{\rm I}\frac{b+3(A_{\rm R}^2+A_{\rm I}^2)}{3(A_{\rm R}^2+A_{\rm I}^2)} > 0$ for which the pair ω_1 and ω_2 have the same (negative) imaginary parts and equal but opposite real parts. The root ω_3 is purely (negative) imaginary. It should be noted that the real and imaginary parts of a root are, respectively, the resonance frequency and the temporal attenuation frequency of the process. The first pair, those with the same negative imaginary part and equal but opposite real parts, correspond to an underdamped harmonic oscillation and they represent torsional waves propagating in opposite directions. The other two roots, the purely (negative) imaginary ω_3 and the trivial root $\omega_4 = 0$ correspond to an overdamped harmonic oscillation and they represent a diffusive torsional process. In the usual nomenclature, the former pair is the fast-wave process and the later pair is the slow-wave process. Clearly if a porous sample is set into torsional resonance, it is the fast process that goes into vibration because only its eigenfrequencies have non-zero real parts.

3.3 Some numerical results

Although the eigenfrequency expressions eqs (9)–(11) are exact, the dependence on the material properties is not transparent in them. In order to gain some insight, we present numerical computations of eigenfrequencies, corresponding to the first harmonics in radial (k_1) and axial (l_1) directions, of the fast and slow processes for a sample of Berea sandstone for a wide range of viscosity values. The physical properties used are listed in Appendix C. The computation with respect to viscosity is motivated by the fact that, in a laboratory setting, torsional experiments are often carried out on the same sample saturated with different fluids. It should be noted that in this calculation, for numerical purposes, the fluid density is kept the same, while the viscosity value is varied. The range of viscosity values may seem unrealistic but they are taken in order to exhibit the entire spectrum of behaviour. The resonance frequency and temporal attenuation frequency plots of the fast process, i.e. the real and imaginary parts of the (either ω_1 or ω_2) eigenfrequency, are shown in Fig. 1 (marked as blue and red curves, respectively). Because the real part of the eigenfrequency, $\Re(\omega)$, is zero for a part of the data, we have plotted attenuation as the imaginary part of the eigenfrequency, $\Im(\omega)$, rather than its usual representation as quality factor Q, which is $\frac{\Re(\omega)}{2\Im(\omega)}$. For clarity, both resonance and temporal attenuation frequencies values are scaled by $\omega_{\rm dry}$, the resonance frequency for the dry-frame. The details about $\omega_{\rm dry}$ are in Appendix D. For the mode under consideration

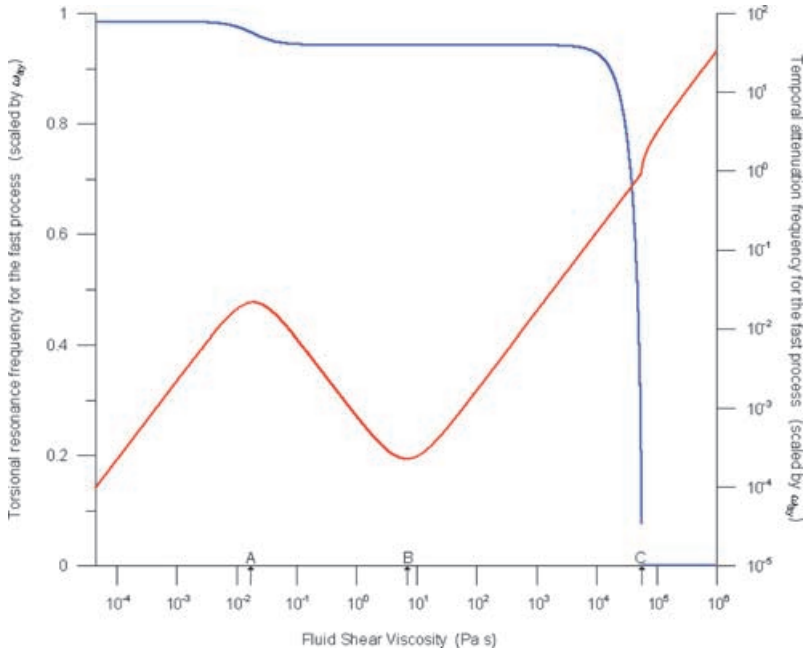

Figure 1. The plot of torsional resonance frequency (blue curve) and temporal attenuation frequency (red curve) versus fluid viscosity associated with the fast process corresponding to the first harmonics in radial and axial directions. Both curves are scaled by the resonance frequency of the dry-frame ($\omega_{\rm dry}$). For clarity the crossover viscosities A, B and C, whose explicit representations are given later in Section 4.3.2, are also marked.

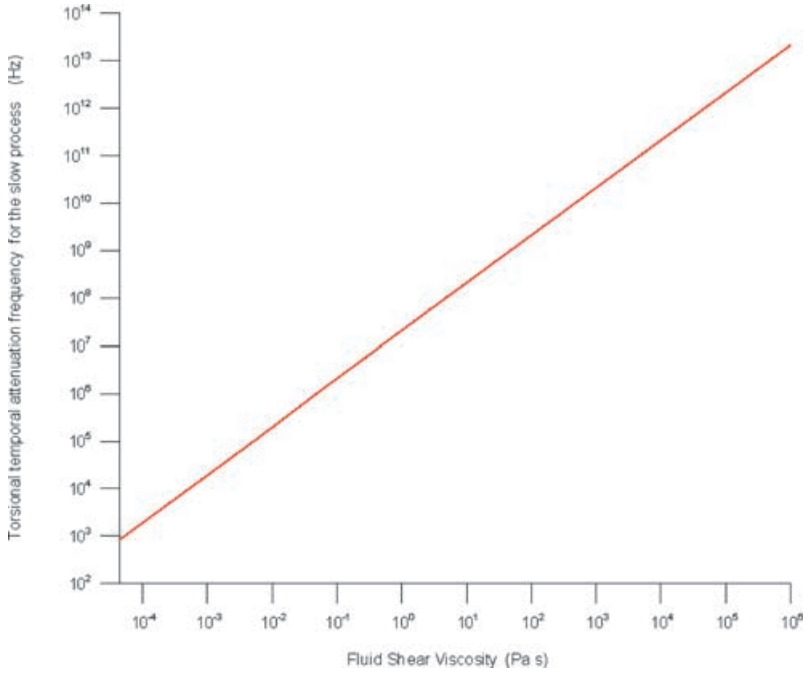

Figure 2. The plot of temporal attenuation frequency versus fluid shear viscosity for the slow process corresponding to the first harmonics in radial and axial directions. In this process the real part of the eigenfrequency is zero, therefore it is not plotted.

its numerical value is 62 kHz. The temporal attenuation frequency curve of the slow process (ω_3) is presented in Fig. 2. In this case the real part of the eigenfrequency is always zero.

The plots in Fig. 1 are characterized by three crossover viscosity values. In the resonance frequency plot the third crossover viscosity, C, marks the transition from an underdamped to an overdamped state of vibration. Above C there is no resonance vibration. Below C there are two regimes defined by the first crossover viscosity marked as A. In each of these two regimes the resonance frequency drops below the value for the dry-frame ($\omega_{\rm dry}$) by constant amounts. The drop is less in the regime that lies below A compared to the regime that lies between A and C. The second crossover viscosity, B, does not have any signature on the resonance plot. The temporal attenuation frequency plot shows segmented linear trends with viscosity. Above the crossover viscosity C, it increases linearly as expected of an overdamped system. Below the crossover viscosity A, the trend is also linearly increasing. At the crossover viscosity A its trend, after forming a smooth crest, becomes linearly decreasing. This trend continues until the crossover viscosity B, at which it again becomes linearly increasing after forming a smooth trough. The temporal attenuation frequency for the slow process presented in Fig. 2 shows the expected increasing linear trend with viscosity.

There are altogether eight material parameters in this problem: four constituent properties, namely, fluid ($\rho_0^{\rm f}$) and solid ($\rho_0^{\rm s}$) mass densities, fluid shear viscosity ($\mu^{\rm f}$) and shear modulus of the solid-grain ($\mu^{\rm s}$); and four averaged parameters, namely, unperturbed porosity (η_0), permeability (K), induced mass coefficient (or tortuosity-factor S) and the frame shear modulus (μ^0). Although in the plots only the variation with respect to fluid viscosity is presented, we find that the variations due to the other parameters do not alter the trends of the curves. A variation in either solid or fluid density simply alters the magnitude of the drop (from the $\omega_{\rm dry}$ value) on the resonance curve. The tortuosity-factor variation only alters the drop value of the resonance frequency curve in the regime below the crossover viscosity A. A change in either frame shear modulus (μ^0) or solid-grain shear modulus ($\mu^{\rm s}$) amounts to a variation in $\omega_{\rm dry}$. Since $\omega_{\rm dry}$ is the scale factor of the resonance frequency plot, the trend of curve remains the same, although, the crossover viscosity A moves to lower values with increasing $\omega_{\rm dry}$. We find that the inverse of permeability has an essentially identical effect on the plots as that of viscosity.

For any given set of material parameters, the numerical computations show their simple dependence on resonance and temporal attenuation frequencies, although in the exact expressions given by eqs (9)–(11) the dependencies are not apparent. In the following section using perturbation theory as applied to eigenvalue problems, we deduce approximate eigenvalues of the operator $\boldsymbol{\mathcal{D}}$ (eq. 4) that are nearly equal to their exact values. We find this procedure renders the approximate expressions for resonance and temporal attenuation frequencies such that the implicit relations with material properties become transparent.

4 THE EIGENVALUE PERTURBATION APPROACH

4.1 The framework

We seek a transformation of the wavefield vector $\mathbf{U} = \mathbf{E}\mathbf{V}$ so that eq. (4) is transformed to

$$\left(\mathbf{I}\frac{d^2}{dt^2} + \boldsymbol{\mathcal{L}}\right)\mathbf{V} = 0, \text{ where } \boldsymbol{\mathcal{L}} \equiv \mathbf{E}^{-1}\boldsymbol{\mathcal{D}}\mathbf{E}. \tag{12}$$

The similarity transformation ensures that the eigenvalue of the resulting transformed operator $\boldsymbol{\mathcal{L}}$ stays the same as that of the operator $\boldsymbol{\mathcal{D}}$. We split the operator $\boldsymbol{\mathcal{L}}$ into its diagonal part $\boldsymbol{\mathcal{L}}^{(0)}$ and off-diagonal part $\mathbf{Q}$, and cast eq. (12) as eigenvalue perturbation problem

$$\left(\mathbf{I}\frac{d^2}{dt^2} + \boldsymbol{\mathcal{L}}^{(0)} + \mathbf{Q}\right)\mathbf{V} = 0, \tag{13}$$

by imposing the transformation matrix $\mathbf{E}$ to be such that:

(1) The eigenvalues of the diagonal part $\boldsymbol{\mathcal{L}}^{(0)}$ of the resulting transformed operator $\boldsymbol{\mathcal{L}}$, given by

$$\left(\mathbf{I}\frac{d^2}{dt^2} + \boldsymbol{\mathcal{L}}^{(0)}\right)\mathbf{V}^{(0)} = 0, \tag{14}$$

are close to the exact eigenvalues of the operator $\boldsymbol{\mathcal{L}}$ (i.e. $\boldsymbol{\mathcal{D}}$), which shall be henceforth referred to as zeroth-order eigenvalues and $\mathbf{V}^{(0)} = \mathbf{E}^{-1}\mathbf{U}$ as zeroth-order eigenvectors.

(2) The perturbations to the zeroth-order eigenvalues due to the off-diagonal part $\mathbf{Q}$ of the transformed operator $\boldsymbol{\mathcal{L}}$ are practically negligible, which is achieved by ensuring the Frobenius norm* of the $\mathbf{Q}$ is orders of magnitude smaller than that of the $\boldsymbol{\mathcal{L}}^{(0)}$.

Hereafter, we shall refer $\boldsymbol{\mathcal{L}}^{(0)}$ and $\mathbf{Q}$ as unperturbed and perturbed operators, respectively. The zeroth-order eigenvalues thus constructed lead to the expressions for resonance and temporal attenuation frequencies in which dominant material properties become distinct.

It turns out the material-parameters space can be split into two regimes. In the first regime the elastic part $\mathbf{W}$ is the dominant piece in the wave operator $\boldsymbol{\mathcal{D}}$ (eq. 4), whereas in the second regime the anelastic parts, $\Omega_{\mathrm{i}}\mathbf{I}_0$ and $\boldsymbol{\nu}$, also become important. A dimensionless parameter, which we have named Υ, marks the boundary of these two regimes. Υ is the ratio of the Darcian dissipation frequency (Ω_{i}) to the resonance frequency of the dry porous frame (ω_{dry}) weighted by a dimensionless parameter (R)

$$\Upsilon = \mathrm{R}\frac{\Omega_{\mathrm{i}}}{\omega_{\mathrm{dry}}}. \tag{15}$$

The explicit expressions of R and Ω_{i} are given in eqs (A7) and (A8), and the formula for ω_{dry} is stated in eq. (D1). Using those it can be expressed in terms of constituent properties as

$$\Upsilon = \frac{1}{2\sqrt{k_p^2 + l_q^2}}\frac{(\frac{\eta_0}{\mathrm{S}})^2}{\sqrt{\phi_0\rho_0^{\mathrm{s}} + \eta_0\rho_0^{\mathrm{f}}\left(1 - \frac{1}{\mathrm{S}}\right)}}\frac{1}{\sqrt{\mu^0}}\frac{\mu^{\mathrm{f}}}{K}. \tag{16}$$

The above suggests that for realistic geomaterials saturated with light fluids, such as air or light hydrocarbon, the likely scenario is $\Upsilon < 10^{-2}$. For low-permeability rocks saturated with water $\Upsilon < 10^{-2}$ still holds true, but for the high-permeability case $10^{-2} < \Upsilon < 1$ is more likely. For heavy hydrocarbons, such as crude oil and tar, $\Upsilon > 1$ is likely to hold true.

The domain $\Upsilon < 1$ pertains to the regime in which the elastic part is dominant and in Fig. 1 it lies below the crossover-viscosity A. The domain $\Upsilon > 1$ corresponds to the regime in which anelastic parts also become important and in Fig. 1 it lies above of the crossover-viscosity A. They can be regarded as inertia dominated and viscosity dominated regimes, respectively. In the following we obtain the transformation matrices corresponding to both regimes, and deduce the expressions for resonance and temporal attenuation frequencies in which dependencies on material properties are transparent.

4.2 Regime I: $\Upsilon < 1$ (inertia dominated regime)

4.2.1 The transformation matrix

In the operator $\boldsymbol{\mathcal{D}}$ (eq. 4), if the viscosity is small, the elastic part $\mathbf{W}$ will be dominant over the anelastic parts, namely, the Darcian dissipation term $\Omega_{\mathrm{i}}\mathbf{I}_0$ and the kinematic viscosity term $\boldsymbol{\nu}$. In this case the transformation $\mathbf{E}^{\mathbf{I}}$ (the superscript$^{\mathrm{I}}$ labels the regime under consideration) should be such that $(\mathbf{E}^{\mathrm{I}})^{-1}\mathbf{W}\mathbf{E}^{\mathrm{I}}$ is a diagonal matrix so that the elastic part, $\mathbf{W}$, is completely incorporated in the diagonal part, $\boldsymbol{\mathcal{L}}^{(0,\mathrm{I})}$, of the transformed operator $\boldsymbol{\mathcal{L}}^{\mathrm{I}}[=(\mathbf{E}^{\mathrm{I}})^{-1}\boldsymbol{\mathcal{D}}\mathbf{E}^{\mathrm{I}}]$ for this regime. The resulting diagonal terms of $(\mathbf{E}^{\mathbf{I}})^{-1}\mathbf{W}\mathbf{E}^{\mathbf{I}}$, i.e. the two eigenvalues of the matrix $\mathbf{W}$ namely ($W^{\mathrm{mm}} + W^{\mathrm{ii}}$) and 0, may be viewed as the two fundamental-frequencies (squared) of the system. Therefore, the transformation matrix $\mathbf{E}^{\mathbf{I}}$ must be the eigenvector matrix of $\mathbf{W}$ and we find it to be

$$\mathbf{E}^{\mathrm{I}} = \frac{1}{1 + \frac{W^{\mathrm{ii}}}{W^{\mathrm{mm}}}}\begin{pmatrix} 1 & -\frac{W^{\mathrm{mi}}}{W^{\mathrm{mm}}} \\ \frac{W^{\mathrm{ii}}}{W^{\mathrm{mi}}} & 1 \end{pmatrix},$$

and using eqs (5) and (A1) it is simplified to

$$= \frac{1}{1 + \varrho_{\mathrm{f}}\mathrm{m}_{\mathrm{f}}}\begin{pmatrix} 1 & -\mathrm{m}_{\mathrm{f}} \\ \varrho_{\mathrm{f}} & 1 \end{pmatrix}. \tag{17}$$

* The Frobenius norm of a matrix $\mathbf{A}$ of order $m \times n$ is $||\mathbf{A}|| = \sqrt{\sum_{i=1}^{m}\sum_{j=1}^{n}|a_{ij}|^2}$, where a_{ij}'s are the elements of the matrix (Golub & Van Loan 1996, Section 2.3).

The entries in the above matrix are dimensionless parameters and they are defined in eqs (A4)–(A6).

The transformed operator $\boldsymbol{\mathcal{L}}^{\mathrm{I}}$ is split into its diagonal $\boldsymbol{\mathcal{L}}^{(0,\mathrm{I})}$ and off-diagonal $\mathbf{Q}^{\mathrm{I}}$ pieces

$$\boldsymbol{\mathcal{L}}^{\mathrm{I}} = (\mathbf{E}^{\mathrm{I}})^{-1}\boldsymbol{\mathcal{D}}\,\mathbf{E}^{\mathrm{I}} = \boldsymbol{\mathcal{L}}^{(0,\mathrm{I})} + \mathbf{Q}^{\mathrm{I}}, \tag{18}$$

where

$$\boldsymbol{\mathcal{L}}^{(0,\mathrm{I})} = \tfrac{1}{1+\varrho_{\mathrm{f}}\mathrm{m_f}}\left[\Omega_{\mathrm{i}}\begin{pmatrix}\varrho_{\mathrm{f}}\mathrm{m_f} & 0\\ 0 & 1\end{pmatrix} + \begin{pmatrix}\nu^{\mathrm{mm}}+\varrho_{\mathrm{f}}\nu^{\mathrm{mi}}+\mathrm{m_f}\nu^{\mathrm{im}}+\varrho_{\mathrm{f}}\mathrm{m_f}\nu^{\mathrm{ii}} & 0\\ 0 & \varrho_{\mathrm{f}}\mathrm{m_f}\nu^{\mathrm{mm}}-\varrho_{\mathrm{f}}\nu^{\mathrm{mi}}-\mathrm{m_f}\nu^{\mathrm{im}}+\nu^{\mathrm{ii}}\end{pmatrix}\right]\tfrac{d}{dt}$$
$$+\begin{pmatrix}W^{\mathrm{mm}}+W^{\mathrm{ii}} & 0\\ 0 & 0\end{pmatrix},$$

and

$$\mathbf{Q}^{\mathrm{I}} = \frac{1}{1+\varrho_{\mathrm{f}}\mathrm{m_f}}\left[\Omega_{\mathrm{i}}\begin{pmatrix}0 & \mathrm{m_f}\\ \varrho_{\mathrm{f}} & 0\end{pmatrix} + \begin{pmatrix}0 & -\mathrm{m_f}\nu^{\mathrm{mm}}+\nu^{\mathrm{mi}}-\mathrm{m_f^2}\nu^{\mathrm{im}}+\mathrm{m_f}\nu^{\mathrm{ii}}\\ -\varrho_{\mathrm{f}}\nu^{\mathrm{mm}}-\varrho_{\mathrm{f}}^2\nu^{\mathrm{mi}}+\nu^{\mathrm{im}}+\varrho_{\mathrm{f}}\nu^{\mathrm{ii}} & 0\end{pmatrix}\right]\frac{d}{dt}.$$

It turns out for the domain $\Upsilon < 1$, the kinematic viscosity terms (ν^{mm} etc.) are orders of magnitude smaller than Ω_{i}, hence, they can be ignored and the unperturbed (or diagonal) part is simply

$$\boldsymbol{\mathcal{L}}^{(0,\mathrm{I})} \approx \frac{\Omega_{\mathrm{i}}}{1+\varrho_{\mathrm{f}}\mathrm{m_f}}\begin{pmatrix}\varrho_{\mathrm{f}}\mathrm{m_f} & 0\\ 0 & 1\end{pmatrix}\frac{d}{dt} + \begin{pmatrix}W^{\mathrm{mm}}+W^{\mathrm{ii}} & 0\\ 0 & 0\end{pmatrix}, \tag{19}$$

and

$$\left(\mathbf{I}\frac{d^2}{dt^2} + \boldsymbol{\mathcal{L}}^{(0,\mathrm{I})}\right)\mathbf{V}^{(0,\mathrm{I})} = 0 \tag{20}$$

yields the eigenvalues that are regarded as zeroth-order. The perturbed (or off-diagonal) part reads

$$\mathbf{Q}^{\mathrm{I}} \approx \frac{\Omega_{\mathrm{i}}}{1+\varrho_{\mathrm{f}}\mathrm{m_f}}\begin{pmatrix}0 & \mathrm{m_f}\\ \varrho_{\mathrm{f}} & 0\end{pmatrix}\frac{d}{dt}. \tag{21}$$

The zeroth-order vector field for this regime is $\mathbf{V}^{(0,\mathrm{I})} = (\mathbf{E}^{\mathrm{I}})^{-1}\mathbf{U}$, and using eq. (A9) in conjunction with eq. (A6) it can be expressed in terms of solid and fluid motions as

$$\mathbf{V}^{(0,\mathrm{I})} = \begin{pmatrix}\mathrm{V}^{(0,\mathrm{I})}_{\mathrm{fast}}\\ \mathrm{V}^{(0,\mathrm{I})}_{\mathrm{slow}}\end{pmatrix} = \begin{pmatrix}1 & \mathrm{m_f}\\ -\varrho_{\mathrm{f}} & 1\end{pmatrix}\begin{pmatrix}\mathrm{U^m}\\ \mathrm{U^i}\end{pmatrix} = \begin{pmatrix}\mathrm{U^s}\\ \frac{\mathrm{S}-1}{\mathrm{S}-\mathrm{m_f}}\mathrm{U^s} - \frac{\mathrm{S}}{\mathrm{S}-\mathrm{m_f}}\mathrm{U^f}\end{pmatrix}. \tag{22}$$

4.2.2 Eigenvalues of the unperturbed operator $\boldsymbol{\mathcal{L}}^{(0,\mathrm{I})}$

(a) Fast Process. From eq. (22) we find the fast process, i.e. the first component of transform field, is simply the solid motion $\mathrm{U^s}$. Naturally the first row of eq. (20) is its governing equation. It is an equation of damped harmonic oscillator. Its dispersion relation yields a frequency pair

$$\omega_1^{(0,\mathrm{I})}, \omega_2^{(0,\mathrm{I})} = -\frac{i}{2}\Omega_{\mathrm{i}}\frac{\varrho_{\mathrm{f}}\mathrm{m_f}}{(1+\varrho_{\mathrm{f}}\mathrm{m_f})} \pm \sqrt{W^{\mathrm{mm}}+W^{\mathrm{ii}} - \left(\frac{\Omega_{\mathrm{i}}}{2}\frac{\varrho_{\mathrm{f}}\mathrm{m_f}}{(1+\varrho_{\mathrm{f}}\mathrm{m_f})}\right)^2},$$

which we regard as the zeroth-order eigenfrequencies of the fast process in the regime I, and we have labelled the superindices of eigenfrequencies accordingly. Obviously, they represent wave processes propagating in opposite directions. Utilizing the expressions of W's (eq. 5 in conjunction with eqs A1 and D1) and Υ (eq. 15) the above is

$$= -\frac{i}{2}\,\Omega_{\mathrm{i}}\frac{\varrho_{\mathrm{f}}\mathrm{m_f}}{(1+\varrho_{\mathrm{f}}\mathrm{m_f})} \pm \omega_{\mathrm{dry}}\sqrt{\mathrm{m_s}\,(1+\varrho_{\mathrm{f}}\mathrm{m_f})}\sqrt{1-\Upsilon^2}.$$

and employing eq. (A6) it is further simplified to

$$\omega_1^{(0,\mathrm{I})}, \omega_2^{(0,\mathrm{I})} = -\frac{i}{2}\Omega_{\mathrm{i}}\frac{\mathrm{m_f}}{\mathrm{S}} \pm \omega_{\mathrm{dry}}\sqrt{\frac{\mathrm{m_s}}{1-\frac{\mathrm{m_f}}{\mathrm{S}}}}\sqrt{1-\Upsilon^2}. \tag{23}$$

The real and (negative) imaginary parts of $\omega_1^{(0,\mathrm{I})}$ (or $\omega_2^{(0,\mathrm{I})}$) are read as zeroth-order resonance and temporal attenuation frequencies for the torsional resonance process. In Fig. 3, superimposed on the respective exact curves, they are plotted as dashed-black lines. The per cent deviation† from their exact values are plotted in Figs 4(a) and (b). These plots show them to be essentially in agreement with the exact values for the viscosity values satisfying the inequality $\Upsilon \ll 1$.

† Per cent deviation = $\frac{\text{approx-exact}}{\text{exact}} \times 100$.

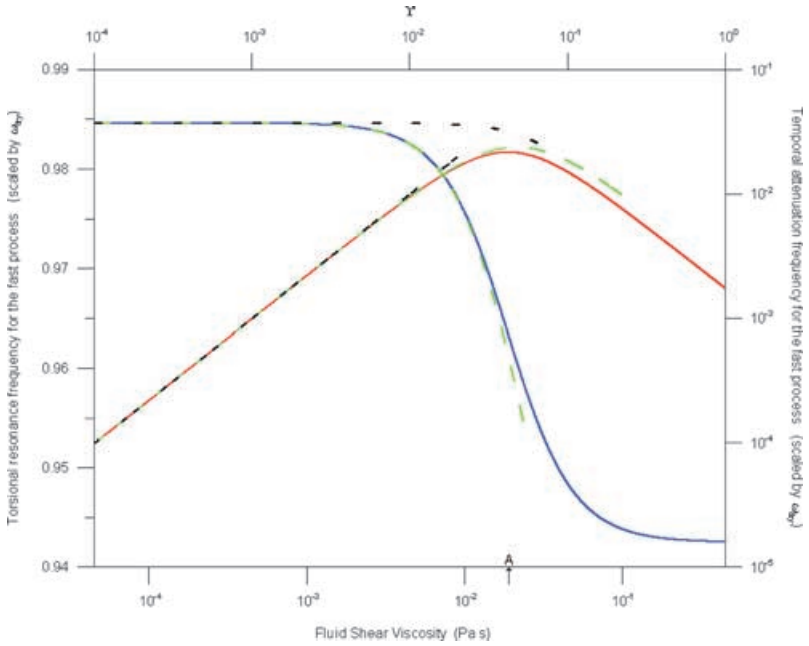

Figure 3. For the regime I ($\Upsilon < 1$) the comparison of exact, zeroth-order, and second-order corrected values of the torsional resonance and temporal attenuation frequencies associated with the fast process. The exact resonance and temporal attenuation frequencies are presented as blue and red curves, respectively. On the respective exact curves, the zeroth-order resonance and temporal attenuation frequencies are superimposed as dashed-black lines, and the dashed-green curves are their second-order corrected values.

In fact for $\Upsilon \ll 1$, the real part of eq. (23), i.e. the resonance frequency, can be approximated as

$$\Re\left(\omega_1^{(0,\mathrm{I})}\right) \approx \omega_{\mathrm{dry}} \sqrt{\frac{\mathrm{m_s}}{1-\frac{\mathrm{m_f}}{\mathrm{S}}}}. \tag{24}$$

We find this approximate resonance frequency expression is valid up to the point where the first flat part of the resonance curve starts bending downwards. For realistic geomaterials saturated with low-viscosity fluids, such as air or light hydrocarbons, Υ is indeed orders of magnitude smaller than unity.

The dimensionless factor $\sqrt{\frac{\mathrm{m_s}}{1-\frac{\mathrm{m_f}}{\mathrm{S}}}}$ can be viewed as the measure of the drop in the value of resonance frequency for wet case over its value for the dry-frame. Obviously this drop factor is controlled by the tortuosity-factor (S) and the fluid-mass fraction.

Using eq. (D1), followed by some algebraic manipulations, eq. (24) can also be viewed as

$$\Re\left(\omega_1^{(0,\mathrm{I})}\right) \approx \sqrt{k_p^2 + l_q^2} \sqrt{\frac{\mu^0}{\phi_0 \rho_0^{\mathrm{s}} + \eta_0 \rho_0^{\mathrm{f}} \left(1-\frac{1}{\mathrm{S}}\right)}}. \tag{25}$$

Thus, controlled by tortuosity-factor, the fluid mass partially participates in the inertia associated with this wave process. The effective density associated with the process is $\phi_0 \rho_0^{\mathrm{s}} + \eta_0 \rho_0^{\mathrm{f}} (1-\frac{1}{\mathrm{S}})$.

Also, utilizing eq. (A8) followed by some algebraic rearrangements, the (negative) imaginary part of eq. (23), i.e. the temporal attenuation frequency can be viewed as

$$-\Im\left(\omega_1^{(0,\mathrm{I})}\right) = \frac{1}{2} \frac{(\frac{\eta_0}{\mathrm{S}})^2}{\phi_0 \rho_0^{\mathrm{s}} + \eta_0 \rho_0^{\mathrm{f}} \left(1-\frac{1}{\mathrm{S}}\right)} \frac{\mu^{\mathrm{f}}}{K}. \tag{26}$$

It is apparent that, here, the temporal attenuation frequency is inversely proportional to fluid mobility (ratio of permeability to fluid viscosity), where the proportionality constant is a function of constituent masses and tortuosity-factor. Also, it is independent of wavenumbers, hence, for different modes the same temporal attenuation will be observed.

For geomaterial saturated with air Υ is likely to be under 10^{-2}, thus, the resonance frequency formula given by eq. (25) is applicable. Since the density of air is over three orders in magnitude smaller than the solid density, hence, contribution of the tortuosity-factor term in eq. (25) is negligible and the resonance frequency for an air-saturated sample is essentially the same as ω_{dry}. Furthermore, eq. (26), on account of shear viscosity of air being in the order of 10^{-5}, predicts practically no temporal attenuation for air-saturated sample. Therefore, in this case if any loss is observed it might be attributed to grain-to-grain friction loss in the solid-frame.

(b) Slow Process. Similarly, we find from eq. (22) the second component of the transform field or slow process to be $-\varrho_{\mathrm{f}} \mathrm{U^m} + \mathrm{U^i}$, which may be viewed as a motion of fluid accompanied by solid-frame, $\frac{\mathrm{S}-1}{\mathrm{S}-\mathrm{m_f}} \mathrm{U^s} - \frac{\mathrm{S}}{\mathrm{S}-\mathrm{m_f}} \mathrm{U^f}$. The second row of eq. (20) gives its eigenfrequency pair which is

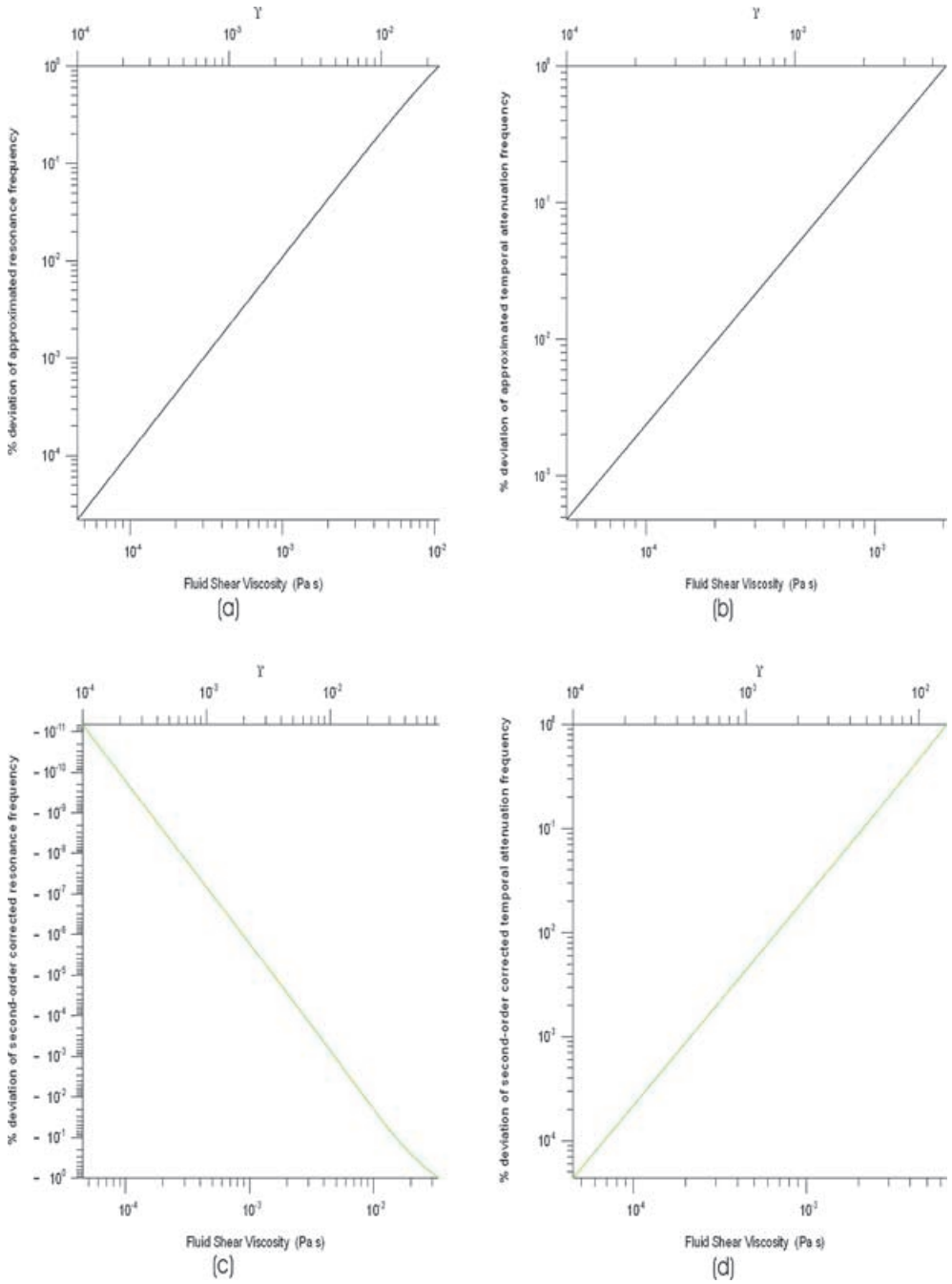

Figure 4. In the regime I ($\Upsilon < 1$) the per cent deviation from the exact values of (a) the zeroth-order resonance frequency, (b) the zeroth-order temporal attenuation frequency, (c) the second-order corrected resonance frequency, and (d) the second-order corrected temporal attenuation frequency associated with the fast process. The deviation curves are monotone functions. On the plots the upper bounds of viscosity (or Υ) correspond to the deviation being 1 per cent.

$$\omega_3^{(0,\mathrm{I})}, \omega_4^{(0,\mathrm{I})} = -i\Omega_\mathrm{i}\frac{1}{1+\varrho_\mathrm{f}\mathrm{m}_\mathrm{f}}, 0 \tag{27}$$

and we regard them as the zeroth-order eigenfrequencies of the slow process in the regime I. The subindex of eigenfrequency is as per notation introduced in Section 3.2. Clearly the first mode, being devoid of a real part, is a diffusive process, and the second is a non-propagating mode. It is almost able to reproduce the temporal attenuation frequency curve for this regime as shown in Fig. 5(a). Its per cent deviation from the exact value is plotted in Fig. 5(b).

4.2.3 The correction due to the perturbation operator $\boldsymbol{Q}^{\mathrm{I}}$

(a) Fast Process. We find that up to the point where viscosity reaches the value so that Ω_i is equal to $\sqrt{W^{\mathrm{ii}}}$, the 2^{nd}-order perturbative correction of $\mathbf{Q}^{\mathrm{I}}$ is able to approximately reproduce the exact graphs as shown in Fig. 3 as dashed-green lines. The per cent deviation from

the exact values are shown in Figs 4(c) and (d). The details about the methodology of the perturbative computation is given in Appendix E. Beyond that point this correction also fails since the perturbation part, $\mathbf{Q}^{\mathrm{I}}$, becomes comparable to the unperturbed part, $\mathcal{L}^{(0,1)}$. It implies that the transformation defined by eq. (17) is no longer valid and, therefore, beyond this point another transformation matrix has to be reworked by incorporating the Ω_i term appropriately.

(b) Slow Process. The zeroth-order curve is essentially in agreement with the exact curve. The correction introduced by carrying the perturbation up to second-order is insignificant, hence for the sake of clarity in Fig. 5 it is not shown.

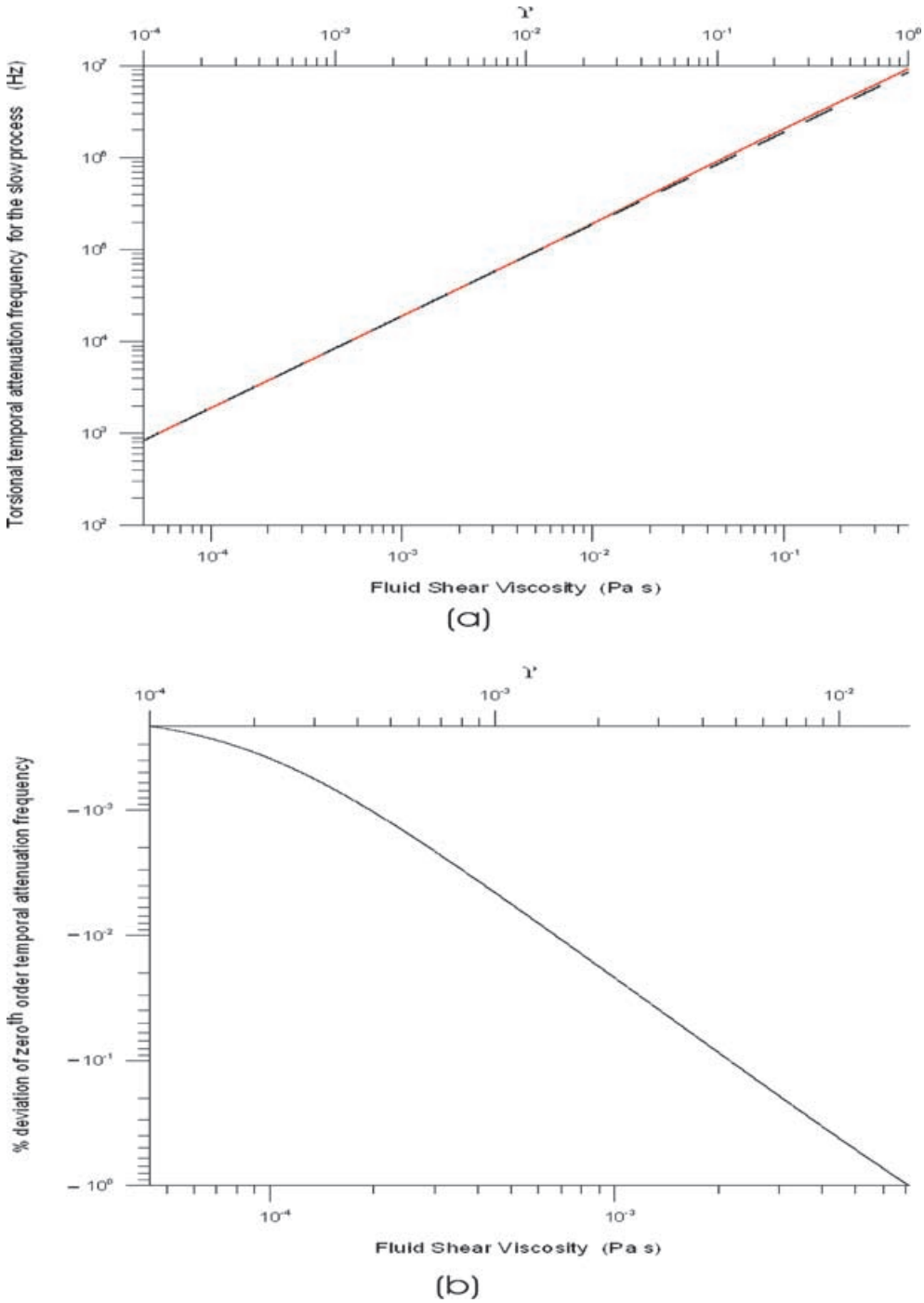

Figure 5. For the regime I ($\Upsilon < 1$) (a) the comparison of the exact (red) and the zeroth-order (dashed-black) values of the temporal attenuation frequency associated with the slow process, and (b) the per cent deviation of the zeroth-order value from the exact value. For clarity, the upper bound of viscosity (or Υ) is taken to be the value by which deviation grows to -1 per cent.

4.3 Regime II: $\Upsilon > 1$ (viscosity dominated regime)

4.3.1 The transformation matrix

The appropriate transformation matrix for this regime turns out to be

$$\mathbf{E}^{\mathrm{II}} = (1-\epsilon)\begin{pmatrix} 1 & \sqrt{\frac{\epsilon}{1-\epsilon}} \\ -\sqrt{\frac{\epsilon}{1-\epsilon}} & 1 \end{pmatrix}. \tag{28}$$

The superscript$^{\mathrm{II}}$ labels the regime and the parameter ϵ is defined as

$$\epsilon = \frac{W^{\mathrm{ii}}}{\Omega_{\mathrm{i}}^2}. \tag{29}$$

It contains viscosity as an inverse squared term, since Ω_{i} is directly proportional to viscosity. Eq. (5) in conjunction with eqs (A1) and (D1) yields W^{ii} to be $\varrho_{\mathrm{f}}\mathrm{m_f m_s}\omega^2_{\mathrm{dry}}$. Using eq. (15) Ω_{i} is expressed in terms of Υ. Thereafter, employing eq. (A6), the above expression is

$$\epsilon = \frac{1}{4}\left(\frac{\mathrm{m_f}}{\mathrm{S}}\right)^3 \frac{1}{\Upsilon^2}. \tag{30}$$

At the lower bound of this regime $\Upsilon = 1$, for which ϵ is $\frac{1}{4}(\frac{\mathrm{m_f}}{\mathrm{S}})^3$ and for a realistic set of geomaterial parameters, turns out to be less than 10^{-2}. With the increment of viscosity, Υ also increases, and hence ϵ dwindles further down ensuring it to be a pertinent perturbative term.

The transformed operator $\boldsymbol{\mathcal{L}}^{\mathrm{II}}$ for this regime is split into its diagonal $\boldsymbol{\mathcal{L}}^{(0,\mathrm{II})}$ and off-diagonal $\mathbf{Q}^{\mathrm{II}}$ pieces as

$$\boldsymbol{\mathcal{L}}^{\mathrm{II}} = (\mathbf{E}^{\mathrm{II}})^{-1}\boldsymbol{\mathcal{D}}\mathbf{E}^{\mathrm{II}} = \boldsymbol{\mathcal{L}}^{(0,\mathrm{II})} + \mathbf{Q}^{\mathrm{II}}, \tag{31}$$

where

$$\begin{aligned}\boldsymbol{\mathcal{L}}^{(0,\mathrm{II})} = &\left[\Omega_{\mathrm{i}}\begin{pmatrix}\epsilon & 0\\ 0 & 1-\epsilon\end{pmatrix}\right.\\ &\left.+\begin{pmatrix}(1-\epsilon)\nu^{\mathrm{mm}} - \sqrt{\epsilon(1-\epsilon)}\nu^{\mathrm{mi}} - \sqrt{\epsilon(1-\epsilon)}\nu^{\mathrm{im}} + \epsilon(1-\epsilon)\nu^{\mathrm{ii}} & 0\\ 0 & \epsilon(1-\epsilon)\nu^{\mathrm{mm}} + \sqrt{\epsilon(1-\epsilon)}\nu^{\mathrm{mi}} + \sqrt{\epsilon(1-\epsilon)}\nu^{\mathrm{im}} + (1-\epsilon)\nu^{\mathrm{ii}}\end{pmatrix}\right]\frac{d}{dt}\\ &+\begin{pmatrix}(1-\epsilon)W^{\mathrm{mm}} - \sqrt{\epsilon(1-\epsilon)}W^{\mathrm{mi}} - \sqrt{\epsilon(1-\epsilon)}W^{\mathrm{im}} + \epsilon(1-\epsilon)W^{\mathrm{ii}} & 0\\ 0 & \epsilon(1-\epsilon)W^{\mathrm{mm}} + \sqrt{\epsilon(1-\epsilon)}W^{\mathrm{mi}} + \sqrt{\epsilon(1-\epsilon)}W^{\mathrm{im}} + (1-\epsilon)W^{\mathrm{ii}}\end{pmatrix},\end{aligned}$$

and

$$\begin{aligned}\mathbf{Q}^{\mathrm{II}} = &\left[\Omega_{\mathrm{i}}\begin{pmatrix}0 & -\sqrt{\epsilon(1-\epsilon)}\\ -\sqrt{\epsilon(1-\epsilon)} & 0\end{pmatrix}\right.\\ &\left.+\begin{pmatrix}0 & \sqrt{\epsilon(1-\epsilon)}\nu^{\mathrm{mm}} + (1-\epsilon)\nu^{\mathrm{mi}} - \epsilon(1-\epsilon)\nu^{\mathrm{im}} - \sqrt{\epsilon(1-\epsilon)}\nu^{\mathrm{ii}}\\ \sqrt{\epsilon(1-\epsilon)}\nu^{\mathrm{mm}} - \epsilon(1-\epsilon)\nu^{\mathrm{mi}} + (1-\epsilon)\nu^{\mathrm{im}} - \sqrt{\epsilon(1-\epsilon)}\nu^{\mathrm{ii}} & 0\end{pmatrix}\right]\frac{d}{dt}\\ &+\begin{pmatrix}0 & \sqrt{\epsilon(1-\epsilon)}W^{\mathrm{mm}} + (1-\epsilon)W^{\mathrm{mi}} - \epsilon(1-\epsilon)W^{\mathrm{im}} - \sqrt{\epsilon(1-\epsilon)}W^{\mathrm{ii}}\\ \sqrt{\epsilon(1-\epsilon)}W^{\mathrm{mm}} - \epsilon(1-\epsilon)W^{\mathrm{mi}} + (1-\epsilon)W^{\mathrm{im}} - \sqrt{\epsilon(1-\epsilon)}W^{\mathrm{ii}} & 0\end{pmatrix}.\end{aligned}$$

Since in this regime the value of ϵ is orders of magnitude smaller than unity, the unperturbed (diagonal) operator $\boldsymbol{\mathcal{L}}^{(0,\mathrm{II})}$ is approximated by dropping such terms as

$$\boldsymbol{\mathcal{L}}^{(0,\mathrm{II})} \approx \left[\Omega_{\mathrm{i}}\begin{pmatrix}\epsilon & 0\\ 0 & 1\end{pmatrix} + \begin{pmatrix}\nu^{\mathrm{mm}} & 0\\ 0 & \nu^{\mathrm{ii}}\end{pmatrix}\right]\frac{d}{dt} + \begin{pmatrix}W^{\mathrm{mm}} & 0\\ 0 & W^{\mathrm{ii}}\end{pmatrix}, \tag{32}$$

and

$$\left(\mathbf{I}\frac{d^2}{dt^2} + \boldsymbol{\mathcal{L}}^{(0,\mathrm{II})}\right)\mathbf{V}^{(0,\mathrm{II})} = 0 \tag{33}$$

yields the eigenvalues that are regarded as zeroth-order. The perturbation (off-diagonal) operator is

$$\mathbf{Q}^{\mathrm{II}} \approx \begin{pmatrix}0 & \nu^{\mathrm{mi}}\\ \nu^{\mathrm{im}} & 0\end{pmatrix}\frac{d}{dt} + \begin{pmatrix}0 & W^{\mathrm{mi}}\\ W^{\mathrm{im}} & 0\end{pmatrix}. \tag{34}$$

The zeroth-order vector field for this regime is

$$\mathbf{V}^{(0,\mathrm{II})} = \begin{pmatrix}\mathrm{V}^{(0,\mathrm{II})}_{\mathrm{fast}}\\ \mathrm{V}^{(0,\mathrm{II})}_{\mathrm{slow}}\end{pmatrix} = \left(\mathbf{E}^{\mathrm{II}}\right)^{-1}\mathbf{U} = \begin{pmatrix}\mathrm{U^m} - \sqrt{\frac{\epsilon}{1-\epsilon}}\mathrm{U^i}\\ \sqrt{\frac{\epsilon}{1-\epsilon}}\mathrm{U^m} + \mathrm{U^i}\end{pmatrix}. \tag{35}$$

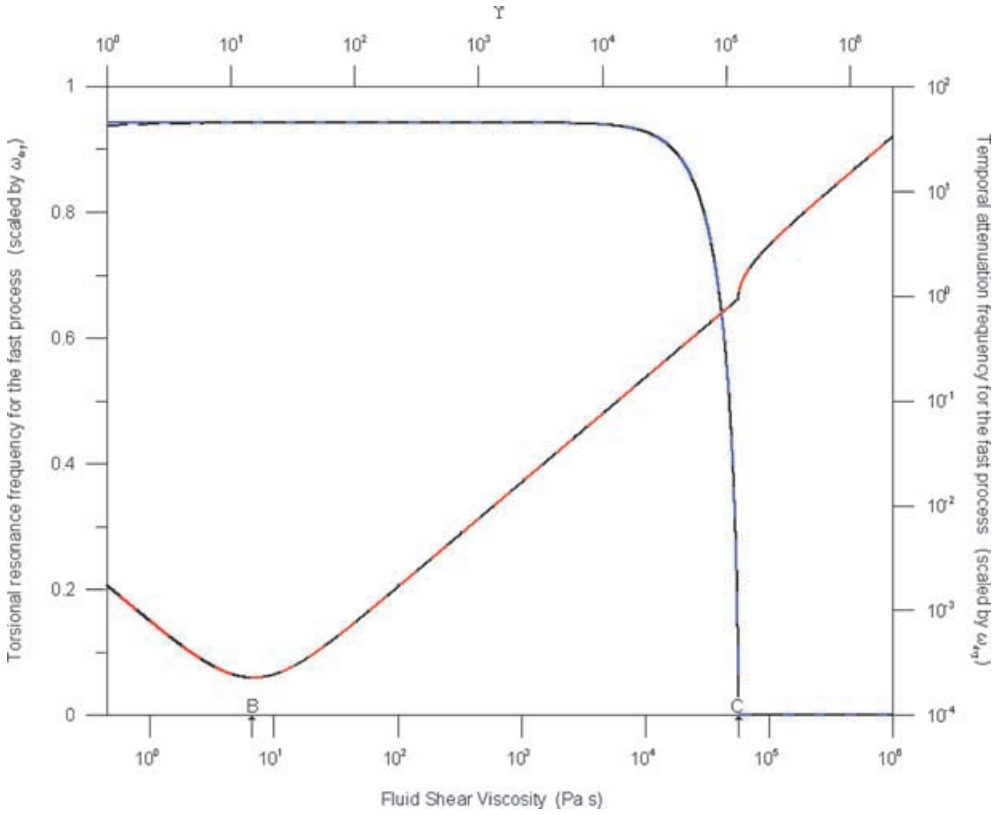

Figure 6. For the regime II ($\Upsilon > 1$) the comparison of the exact and zeroth-order values of the torsional resonance and temporal attenuation frequencies associated with the fast process. The blue and red curves are the exact resonance and temporal attenuation frequencies, respectively. The superimposed dashed-black curves on the respective exact curves are the zeroth-order values.

4.3.2 Eigenvalues of the unperturbed operator $\mathcal{L}_0^{\mathrm{II}}$

(a) Fast Process. It is obvious from the first row of eq. (35) that in this regime the fast process is basically centre-of-mass motion (U^{m}), and the difference motion of the solid and fluid constituents (U^{i}) is inconsequential. The first row of eq. (33) is its governing equation that yields the eigenvalues for the process as

$$\omega_1^{(0,\mathrm{II})}, \omega_2^{(0,\mathrm{II})} = -\frac{i}{2}\left(\epsilon\Omega_{\mathrm{i}} + \nu^{\mathrm{mm}}\right) \pm \sqrt{W^{\mathrm{mm}} - \left[\frac{1}{2}\left(\epsilon\Omega_{\mathrm{i}} + \nu^{\mathrm{mm}}\right)\right]^2}. \tag{36}$$

The real and (negative) imaginary parts of $\omega_1^{(0,\mathrm{II})}$(or $\omega_2^{(0,\mathrm{II})}$) are read as zeroth-order resonance and temporal attenuation frequencies for the torsional resonance process. In Fig. 6, superimposed on the respective exact curves, they are plotted as dashed-black lines. The per cent deviation from their exact values are plotted in Figs 7(a) and (b), which show them to be in good agreement.

Just prior to the crossover viscosity C, for which in Fig. 6 the resonance curve is flat, the inequality $W^{\mathrm{mm}} \gg [\frac{1}{2}(\epsilon\Omega_{\mathrm{i}} + \nu^{\mathrm{mm}})]^2$ holds true. It suggests that for this region the resonance frequency, i.e. the real part of $\omega_1^{(0,\mathrm{II})}$, can be approximated as

$$\Re\left(\omega_1^{(0,\mathrm{II})}\right) \approx \sqrt{W^{\mathrm{mm}}},$$

and using eq. (5) in conjuction with eqs (A1) and (D1) it is simplified to

$$= \omega_{\mathrm{dry}}\sqrt{\mathrm{m_s}} = \sqrt{k_p^2 + l_q^2}\sqrt{\frac{\mu^0}{\rho_0^{\mathrm{m}}}}. \tag{37}$$

We find this approximate resonance frequency expression is valid up to the point (prior to the crossover viscosity C) where the flat part of the resonance curve starts bending downwards. From the first row of eqs (35) and (37) it is apparent that here the wave motion is essentially unison vibration of solid-frame and pore fluid, such that the fluid imparts its mass completely to the inertia associated with the process. Hence, it is the total density, ρ_0^{m}, that is associated with this process. As opposed to the regime I, here, the drop factor of the value of (wet) resonance frequency with respect to ω_{dry} is independent of the tortuosity-factor.

Since ϵ is $\frac{W^{\mathrm{ii}}}{\Omega_{\mathrm{i}}^2}$, the term $\epsilon\Omega_{\mathrm{i}}$ is inversely proportional to viscosity, whereas the term ν^{mm} is directly proportional to viscosity. At the viscosity value for which $\Omega_{\mathrm{i}} = \frac{W^{\mathrm{ii}}}{\nu^{\mathrm{mm}}}$ holds true, these two terms become equal. This viscosity value precisely corresponds to the crossover

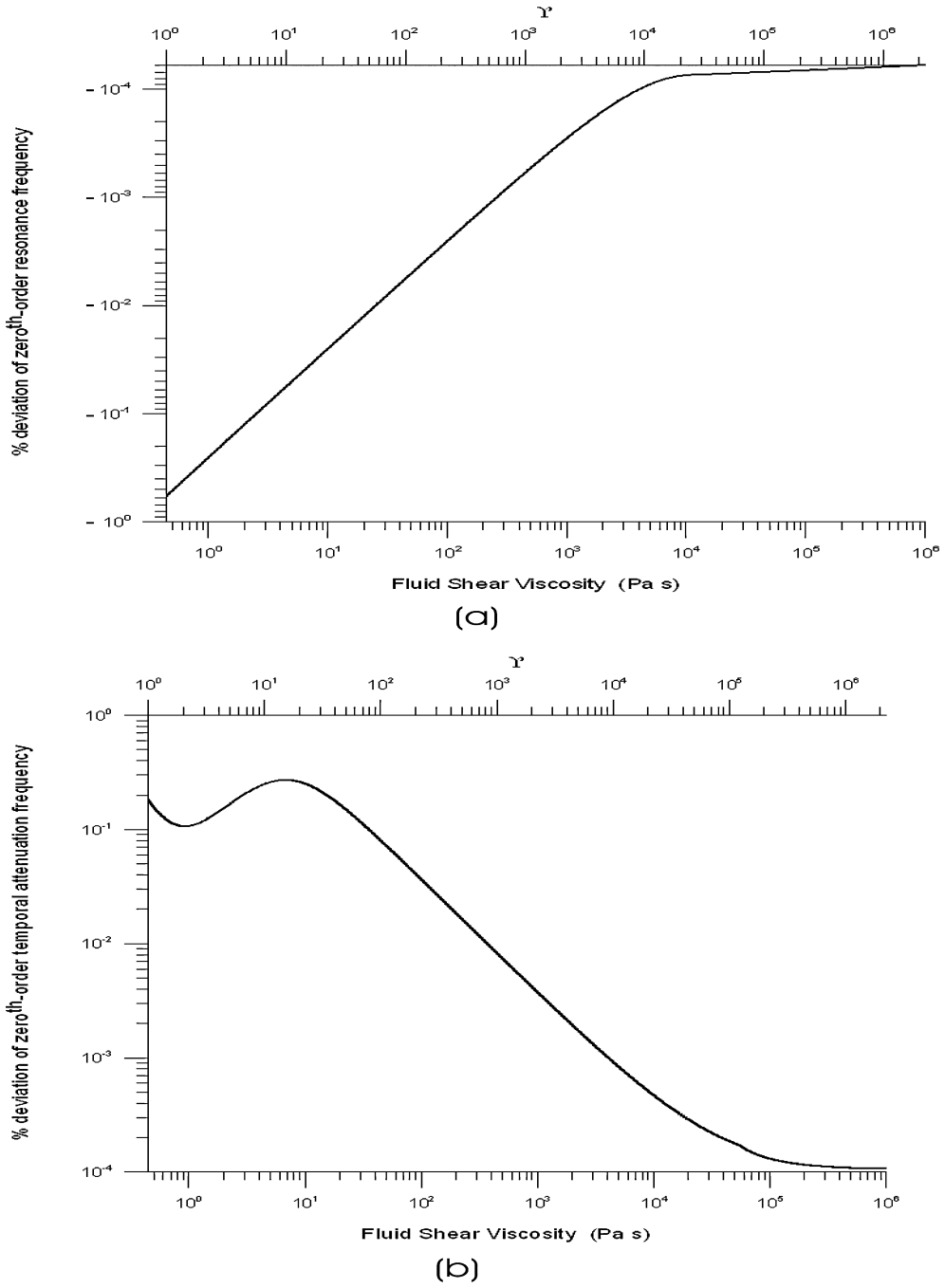

Figure 7. For the regime II ($\Upsilon > 1$) the per cent deviation from the exact values of (a) the zeroth-order resonance frequency, and (b) the zeroth-order temporal attenuation frequency associated with the fast process.

viscosity B. For lower viscosity values, the temporal attenuation frequency for the fast process, i.e. (negative) imaginary part of $\omega_1^{(0,\mathrm{II})}$, is simply dominated by $\epsilon\Omega_\mathrm{i}$. Whereas, for higher viscosity values attenuation is dominated by ν^{mm}.

Thus, in the region between A and B, the approximate formula for temporal attenuation of the fast process is

$$-\Im\left(\omega_1^{(0,\mathrm{II})}\right) \approx \frac{\epsilon\Omega_\mathrm{i}}{2},$$

and using eq. (30) together with eqs (15), (A6), (A7) and (D1) it is re-expressed as

$$= \frac{k_p^2 + l_q^2}{2}\left(\frac{\rho_0^\mathrm{f}}{\rho_0^\mathrm{m}}\right)^2 \mu^0 \frac{K}{\mu^\mathrm{f}}. \tag{38}$$

In contrast to regime I, here, the temporal attenuation frequency is wavenumber dependent and is directly proportional to fluid mobility where the proportionality constant is a function of constituent masses and frame shear modulus.

It should be noted that the intersection of eqs (26) and (38) defines the crossover viscosity A. It turns out to be the point where the viscosity value is such that $\sqrt{W^{\rm mm}+W^{\rm ii}}=\Omega_{\rm i}$ holds true.

For the region between B and C the approximate formula for temporal attenuation of the fast process is

$$-\Im\left(\omega_1^{(0,\rm II)}\right)\approx\frac{\nu^{\rm mm}}{2},$$

and employing eq. (6) in conjunction with eq. (A2) it amounts to

$$=\frac{k_p^2+l_q^2}{2}\left(1-\frac{\mu^0}{\mu^{\rm s}}\right)\frac{1}{\rho_0^{\rm m}}\mu^{\rm f}. \tag{39}$$

The crossover viscosity C marks the transition from an underdamped to an overdamped state of vibration. It is the point where the viscosity value is such that $\sqrt{W^{\rm mm}}=\frac{1}{2}(\epsilon\Omega_{\rm i}+\nu^{\rm mm})\approx\frac{1}{2}\nu^{\rm mm}$ (since $\epsilon\Omega_{\rm i}\ll\nu^{\rm mm}$) holds true. Beyond the point C the resonance frequency is zero and the expression for temporal attenuation frequency can be approximated as

$$\begin{aligned}-\Im\left(\omega_1^{(0,\rm II)}\right)&\approx\epsilon\Omega_{\rm i}+\nu^{\rm mm}\\&\approx\nu^{\rm mm}=\left(k_p^2+l_q^2\right)\left(1-\tfrac{\mu^0}{\mu^{\rm s}}\right)\tfrac{1}{\rho_0^{\rm m}}\mu^{\rm f}.\end{aligned} \tag{40}$$

It should be noted that for realistic geomaterials, parameters are normally such that regime wherein eq. (40) becomes applicable is never reached, however, for the sake of completeness of the analysis this was also calculated.

(b) Slow Process. From the second row of eq. (35) we find the slow wave to be basically difference motion of phases ($U^{\rm i}$) with very insignificant amount of centre-of-mass motion ($U^{\rm m}$), therefore, it can be regarded as a fluid flow process. The second row of eq. (33) gives its eigenfrequency pair, which is

$$\omega_3^{(0,\rm II)},\omega_4^{(0,\rm II)}=-\frac{i}{2}\left(\Omega_{\rm i}+\nu^{\rm ii}\right)\pm\sqrt{W^{\rm ii}-\left[\frac{1}{2}\left(\Omega_{\rm i}+\nu^{\rm ii}\right)\right]^2}.$$

Taking into consideration that here $\sqrt{W^{\rm ii}}\ll\frac{\Omega_{\rm i}+\nu^{\rm ii}}{2}$, we have

$$\omega_3^{(0,\rm II)},\omega_4^{(0,\rm II)}\approx-i\left(\Omega_{\rm i}+\nu^{\rm ii}\right),-i\frac{W^{\rm ii}}{\Omega_{\rm i}+\nu^{\rm ii}}. \tag{41}$$

We regard $\Omega_{\rm i}+\nu^{\rm ii}$ to be the zeroth-order temporal attenuation frequency associated with the slow-wave. It is almost able to reproduce the exact temporal attenuation frequency curve for the slow-wave in this regime as shown in Fig. 8(a). The per cent deviation from its exact value is plotted in Fig. 8(b). The additional diffusive process with temporal attenuation frequency $\frac{W^{\rm ii}}{\Omega_{\rm i}+\nu^{\rm ii}}$ tends to be a non-propagating mode with increasing viscosity.

4.3.3 The correction due to the perturbation operator $\boldsymbol{Q}^{II}$

For both processes, fast as well as slow, we find that the corrections introduced by carrying the perturbation up to second order are insignificant and as the zeroth-order curves are essentially in agreement with the exact curves, for the sake of clarity in Figs 6 and 8(a) we have chosen not to plot them.

5 CONCLUSIONS

In the framework of the volume-averaged theory of poroelasticity we have carried out the complete analysis of the standing torsional waves in a finite fully-saturated, porous, circular cylinder. We have shown that an underdamped harmonic oscillation (i.e. a propagating-wave process or fast process) and an overdamped harmonic oscillation (i.e. a diffusive process) constitute the eigenprocesses of the governing 2×2 matrix wave equation. It is the former process that is observed in a torsional-resonance experiment.

In order to gain insight into the nature of the eigenvectors and eigenvalues of this problem, we have carried out eigenvalue perturbation analysis. The set of two similarity transformations that allowed the construction of nearly exact eigenvalues have been vital to this analysis. It led to expressions of torsional resonance and temporal attenuation frequencies in which links to the constituent properties are transparent. It showed that entire material-parameters space can be split into two regimes, namely, inertia dominated and viscosity dominated. The domain of two regimes is found to be defined by the parameter Υ (eq. 15): the domain $\Upsilon<1$ corresponds to former and the domain $\Upsilon>1$ is associated with later.

For sandstones or limestones saturated with light fluids, such as air or light hydrocarbon, we found $\Upsilon\ll1$, therefore, the expressions for torsional resonance (eq. 25) and temporal attenuation (eq. 26) frequencies pertaining to inertia dominated regime are applicable here. For heavy hydrocarbons, such as crude oil and tar, $\Upsilon>1$ holds true suggesting the expressions for the torsional resonance (eq. 37) and temporal attenuation (eqs 38 or 39) frequencies corresponding to the viscosity dominated regime are pertinent here.

Based upon this work we have a firm basis to design a variety of torsional oscillation experiments to determine frame shear modulus, permeability, and tortuosity-factor.

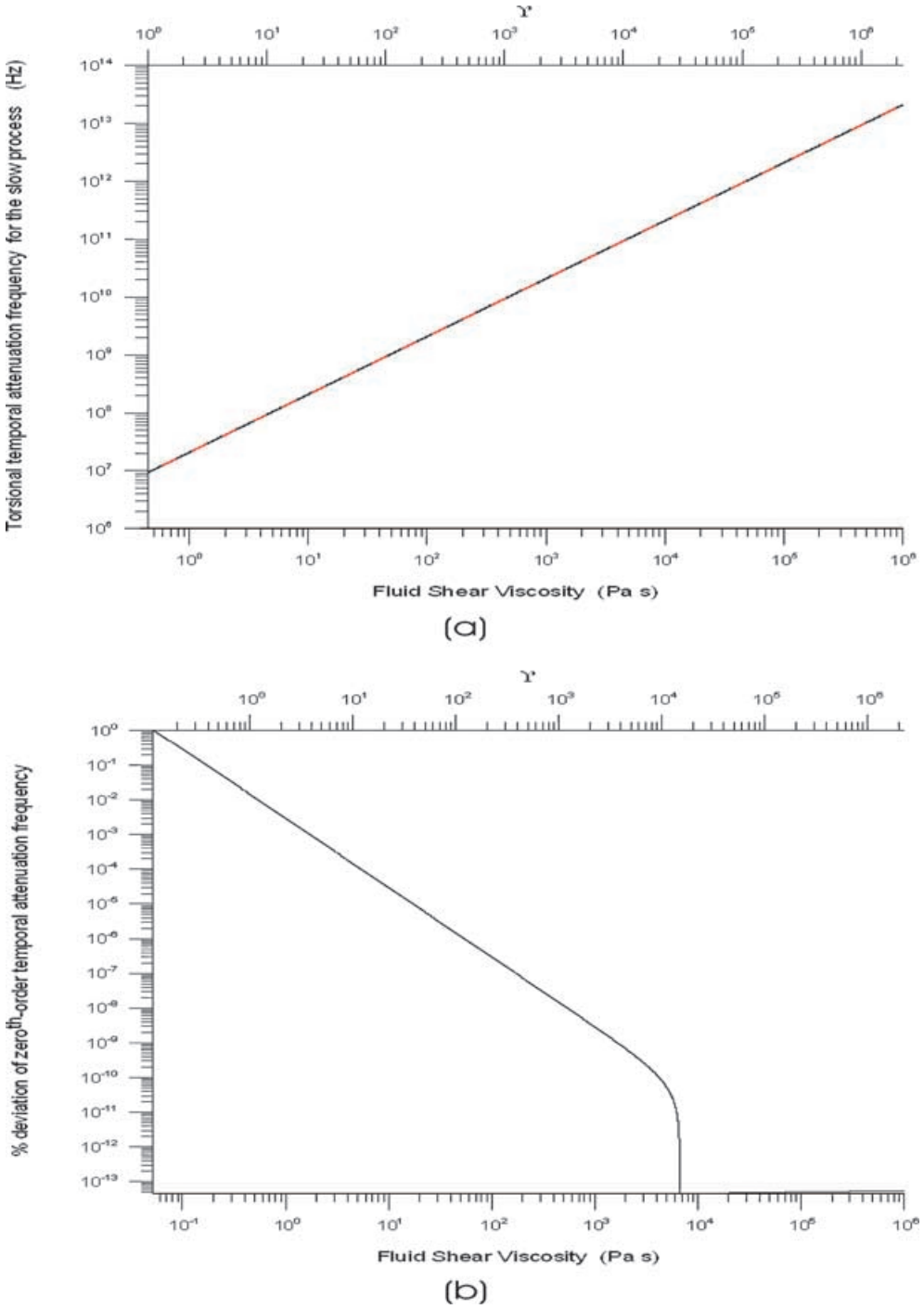

Figure 8. For the regime II ($\Upsilon > 1$) (a) the comparison of the exact (red) and zeroth-order (dashed-black) values of the temporal attenuation frequency associated with the slow process, and (b) the per cent deviation of the zeroth-order value from the exact value.

ACKNOWLEDGMENTS

The authors are grateful to the reviewers for their comments, which helped to improve the clarity of the paper. This work was supported by CICESE project #641113, and CONACyT grants #32663-T and #39387-T. SS was supported through the CONACyT studentship # 118209.

REFERENCES

Biot, M.A., 1956. Theory of propagation of elastic waves in a fluid-saturated porous solid. I. low-frequency range, *J. acoust. Soc. Am.,* **28**(2), 168–178.
Biot, M.A., 1962. Mechanics of deformation and acoustic propagation in porous media, *J. appl. Phys.,* **33**(4), 1482–1492.
Bourbie, T., Coussy, O. & Zinszner, B., 1987. *Acoustic of Porous Media,* Gulf Publishing Company. Houston, TX, USA.

de la Cruz, V. & Spanos, T.J.T., 1985. Seismic wave propagation in a porous medium, *Geophysics,* **50**(10), 1556–1565.
de la Cruz, V. & Spanos, T.J.T., 1989. Thermomechanical coupling during seismic wave propagation in a porous medium, *J. geophys. Res.,* **94**(B), 637–642.
de la Cruz, V., Sahay, P.N. & Spanos, T.J.T., 1993. Thermodynamic of porous media, *Proc. R. Soc. Lond. A.,* **433**, 247–255.
Dunn, K.J., 1986. Acoustic attenuation in fluid-saturated porous cylinders at low frequencies, *J. acoust. Soc. Am.,* **79**(6), 1709–1721.
Golub, G. & Van Loan, C.F., 1996. *Matrix Computations,* The John Hopkins University Press, Baltimore, MD, USA.
Hickey, C.J., Spanos, T.J.T. & de la Cruz, V., 1995. Deformation parameters of permeable media, *Geophys. J. Int.,* **121**, 359–370.
Morse, P.M. & Feshbach, H., 1953. *Methods of Theoretical Physics,* **2**, McGraw-Hill, New York, NY, USA.
O'Hara, S.G., 1985. Influence of pressure, temperature, and pore fluid on the frequency-dependent attenuation of elastic waves in Berea sandstone, *Phys. Rev. A.,* **32**(1), 472–488.
Sahay, P.N., 1996. Elastodynamics of deformable Porous Media, *Proc. R. Soc. Lond.,* **452**, 1517–1529.
Sahay, P.N., Spanos, T.J.T. & de la Cruz, V., 2001. Seismic wave propagation in inhomogeneous and anisotropic porous media, *Geophys. J. Int.,* **145**, 209–222.
Sahay, P.N., 2001. Biot theory, BISQ model and porosity perturbation during deformation, in *75th. Ann. Internat. Mtg., Soc. Expl. Geophys.,* pp. 1752–1755, expanded abstracts.
Selby, S.M., 1971. *CRC standard mathematical tables,* 19th edn, The Chemical Rubber Co., Cleveland, OH, USA
Sothcott, J., McCann, C. & O'Hara, S.G., 2000. The influence of two different pore fluids on the acoustic properties of reservoir sandstones at sonic and ultrasonic frequencies, in *74th Ann. Internat. Mtg.*, *Soc. Expl. Geophys.,* pp. 1883–1886, expanded abstracts.

APPENDIX A: COEFFICIENTS

The expressions for the coefficients of the equations of motion eq. (1) are obtained in terms of the constituents material properties in a straightforward manner from the appendix of Sahay (1996). We have

$$\mathbf{C} = \begin{pmatrix} C^{mm} & C^{mi} \\ C^{im} & C^{ii} \end{pmatrix} = \begin{pmatrix} 1 & m_f \\ \varrho_f & m_f \varrho_f \end{pmatrix} m_s c_{dry}^2 \tag{A1}$$

$$\mathbf{N} = \begin{pmatrix} N^{mm} & N^{mi} \\ N^{im} & N^{ii} \end{pmatrix} = \begin{bmatrix} 1 + \frac{\phi_0}{\eta_0}\delta^\mu & -\left(m_s - m_f \frac{\phi_0}{\eta_0}\delta^\mu\right) \\ -\varrho_s\left(1 + \frac{\phi_0}{\eta_0}\delta^\mu\right) & \varrho_s\left(m_s - m_f \frac{\phi_0}{\eta_0}\delta^\mu\right) \end{bmatrix} m_f \nu^f \tag{A2}$$

$$\mathbf{I} = \begin{pmatrix} 1 & 0 \\ 0 & 1 \end{pmatrix}$$

$$\mathbf{I}_0 = \begin{pmatrix} 0 & 0 \\ 0 & 1 \end{pmatrix}$$

where

η_0	unperturbed porosity
$\phi_0 = 1 - \eta_0$	solid-volume fraction
ρ_0^s	solid density
ρ_0^f	fluid density
μ^s	solid-grain shear modulus
μ^f	fluid shear viscosity
δ^μ	shear modulus modifier
$\mu^0 = \phi_0 \mu^s (1 - \delta^\mu)$	solid-frame shear modulus
K	permeability
S	tortuosity-factor (structure factor)
$\rho^{12} = -(S-1)\eta_0 \rho_0^f$	induced mass coefficient
$c_{dry}^2 = \frac{\mu^0}{\phi_0 \rho_0^s}$	dry-frame wave speed (squared)
$\nu^f = \frac{\mu^f}{\rho_0^f}$	kinematic viscosity of the fluid

$\rho_0^m = \phi_0\rho_0^s + \eta_0\rho_0^f$ total density

$\frac{1}{\rho_0^r} = \frac{1}{\phi_0\rho_0^s} + \frac{1}{\eta_0\rho_0^f}$ reciprocal of the reduced density

$\rho_0^i = \rho_0^r - \rho^{12} = \rho_0^r\left(1 + \frac{S-1}{m_s}\right)$ modified reduced density

$$m_s = \frac{\phi_0\rho_0^s}{\rho_0^m} \quad \text{solid-mass fraction} \tag{A3}$$

$$m_f = \frac{\eta_0\rho_0^f}{\rho_0^m} \quad \text{fluid-mass fraction} \tag{A4}$$

$$\varrho_s = \frac{\phi_0\rho_0^s}{\rho_0^i} = \frac{\rho_0^m}{\rho_0^i}m_s = \frac{m_s}{m_f}\frac{1}{S - m_f} \tag{A5}$$

$$\varrho_f = \frac{\eta_0\rho_0^f}{\rho_0^i} = \frac{\rho_0^m}{\rho_0^i}m_f = \frac{1}{S - m_f} \tag{A6}$$

$$R = \frac{\varrho_f m_f}{2\sqrt{m_s}(1 + \varrho_f m_f)^{3/2}} = \frac{m_f}{2S}\left(\frac{1 - \frac{m_f}{S}}{m_s}\right)^{1/2} \tag{A7}$$

$$\begin{aligned}\Omega_i &= \frac{\eta_0^2\mu^f}{\rho_0^i K} && \text{Darcian flow relaxation frequency}\\ &= \frac{\eta_0\rho_0^f}{\rho_0^i}\frac{\eta_0\mu^f}{\rho_0^f K} && = \varrho_f \times \text{Biot critical frequency.}\end{aligned} \tag{A8}$$

The U^m and U^i fields in terms of the solid and fluid motions, U^s and U^f respectively, are

$$\begin{pmatrix} U^m \\ U^i \end{pmatrix} = \begin{pmatrix} m_s & m_f \\ 1 & -1 \end{pmatrix}\begin{pmatrix} U^s \\ U^f \end{pmatrix}. \tag{A9}$$

APPENDIX B: STRESSES

$$\sigma_{r\theta}^m = \rho_0^m\left(C^{mm} + N^{mm}\frac{\partial}{\partial t}\right)r\frac{\partial}{\partial r}\left(\frac{u^m}{r}\right) + \rho_0^m\left(C^{mi} + N^{mi}\frac{\partial}{\partial t}\right)r\frac{\partial}{\partial r}\left(\frac{u^i}{r}\right) \tag{B1}$$

$$\sigma_{r\theta}^i = \rho_0^i\left(C^{im} + N^{im}\frac{\partial}{\partial t}\right)r\frac{\partial}{\partial r}\left(\frac{u^m}{r}\right) + \rho_0^i\left(C^{ii} + N^{ii}\frac{\partial}{\partial t}\right)r\frac{\partial}{\partial r}\left(\frac{u^i}{r}\right) \tag{B2}$$

$$\sigma_{\theta z}^m = \rho_0^m\left(C^{mm} + N^{mm}\frac{\partial}{\partial t}\right)\frac{\partial u^m}{\partial z} + \rho_0^m\left(C^{mi} + N^{mi}\frac{\partial}{\partial t}\right)\frac{\partial u^i}{\partial z} \tag{B3}$$

$$\sigma_{\theta z}^i = \rho_0^i\left(C^{im} + N^{im}\frac{\partial}{\partial t}\right)\frac{\partial u^m}{\partial z} + \rho_0^i\left(C^{ii} + N^{ii}\frac{\partial}{\partial t}\right)\frac{\partial u^i}{\partial z} \tag{B4}$$

APPENDIX C: DATA

The following data are used in the numerical computation:

$\rho_0^s = 2.65 \times 10^{+03}$ $\left(\frac{kg}{m^3}\right)$

$\mu^s = 2.30 \times 10^{+10}$ (Pa)

$\rho_0^f = 1.00 \times 10^{+03}$ $\left(\frac{kg}{m^3}\right)$

$\mu^0 = 7.17 \times 10^{+09}$ (Pa)

$K = 1.00 \times 10^{-11}$ (m^2)

$\eta_0 = 0.25$

$S = 4/3$

$a = 2.5 \times 10^{-2}$ (m) radius of the cylindrical core

$H = 40 \times 10^{-2}$ (m) length of the cylindrical core.

APPENDIX D: TORSIONAL RESONANCE FREQUENCY OF THE DRY SOLID FRAME

Below we present the expression of the torsional resonance frequency for a porous frame devoid of fluid. In this case the equation of motion is

$$\phi_0 \rho_0^{\mathrm{s}} \frac{\partial u^{\mathrm{s}}}{\partial t^2} = \mu^0 \left[\frac{1}{r} \frac{\partial}{\partial r} \left(r \frac{\partial}{\partial r} \right) + \frac{\partial^2}{\partial z^2} - \frac{1}{r^2} \right] u^{\mathrm{s}}.$$

Its solution, subjected to the stress-free boundary conditions on the radial surface ($r = a$) as well as on the top ($z = \mathrm{H}$) and bottom ($z = 0$) end-caps, is

$$u^{\mathrm{s}} = \sum_{p=1}^{\infty} \sum_{q=1}^{\infty} B(k_p, l_q) k_p J_1(k_p r) \cos(l_q z) \cos[\omega_{\mathrm{dry}}(k_p, l_q) t],$$

where the radial, k_p, and the axial, l_q, wavenumbers are the same as defined in Section 3.1 and $B(k_p, l_q)$ is a constant to be determined by the initial conditions. The torsional resonance frequency, ω_{dry}, is dependent only on the frame shear modulus and solid-mass density

$$\omega_{\mathrm{dry}}^2 = \left(k_p^2 + l_q^2 \right) \frac{\mu^0}{\phi_0 \rho_0^{\mathrm{s}}}. \tag{D1}$$

APPENDIX E: EIGENVALUE PERTURBATION COMPUTATIONS

For the clarity of this computation, the eigenvalue perturbation problem that is casted in Section 4 as a 2×2 system of second-order ODEs is rewritten as a system of first-order ODEs.

The unperturbed and perturbed operators pertaining to the regime I are re-expressed as 3×3 matrix operators

$$\boldsymbol{\mathcal{L}}^{(0,\mathrm{I})} = \begin{bmatrix} 0 & i & 0 \\ -i\left(W^{\mathrm{mm}} + W^{\mathrm{ii}}\right) & -i\frac{\mathrm{m_f}\varrho_{\mathrm{f}}}{1+\mathrm{m_f}\varrho_{\mathrm{f}}}\Omega_{\mathrm{i}} & 0 \\ 0 & 0 & -i\frac{1}{1+\mathrm{m_f}\varrho_{\mathrm{f}}}\Omega_{\mathrm{i}} \end{bmatrix},$$

$$\mathbf{Q}^{\mathrm{I}} = \begin{pmatrix} 0 & 0 & 0 \\ 0 & 0 & -i\frac{\mathrm{m_f}}{1+\mathrm{m_f}\varrho_{\mathrm{f}}}\Omega_{\mathrm{i}} \\ 0 & -i\frac{\varrho_{\mathrm{f}}}{1+\mathrm{m_f}\varrho_{\mathrm{f}}}\Omega_{\mathrm{i}} & 0 \end{pmatrix},$$

and for the regime II, they are 4×4 matrix operators

$$\boldsymbol{\mathcal{L}}^{(0,\mathrm{II})} = \begin{bmatrix} 0 & 0 & i & 0 \\ 0 & 0 & 0 & i \\ -iW^{\mathrm{mm}} & 0 & -i\left(\epsilon\Omega_{\mathrm{i}} + \nu^{\mathrm{mm}}\right) & 0 \\ 0 & -iW^{\mathrm{ii}} & 0 & -i\left(\Omega_{\mathrm{i}} + \nu^{\mathrm{ii}}\right) \end{bmatrix},$$

$$\mathbf{Q}^{\mathrm{II}} = \begin{pmatrix} 0 & 0 & 0 & 0 \\ 0 & 0 & 0 & 0 \\ 0 & -iW^{\mathrm{mi}} & 0 & -i\nu^{\mathrm{mi}} \\ -iW^{\mathrm{im}} & 0 & -i\nu^{\mathrm{im}} & 0 \end{pmatrix}.$$

The unperturbed problem, with eigenvalues $\omega_{\mathrm{n}}^{(0)}$ and eigenvectors $\mathbf{V}_{\mathrm{n}}^{(0)}$, is given by

$$\boldsymbol{\mathcal{L}}^{(0)} \mathbf{V}_{\mathrm{n}}^{(0)} = \omega_{\mathrm{n}}^{(0)} \mathbf{V}_{\mathrm{n}}^{(0)}.$$

The second superindex labelling the regime is suppressed for clarity of the notation. The subindex n (n = 1, N) labels the modes. N assumes the value 3 and 4, respectively, for the regimes I and II.

$\omega_{\mathrm{n}}^{(0)}$ and $\mathbf{V}_{\mathrm{n}}^{(0)}$ are regarded as the zeroth-order eigenvalues and eigenvectors, respectively, of the operator $\boldsymbol{\mathcal{L}}^{(0)} + \mathbf{Q}$.

The perturbative correction to the zeroth-order eigenvalues and eigenvectors due to the operator $\mathbf{Q}$ is developed following Morse & Feshbach (1953, section 9.1, p. 1018). The iterative expressions of kth-order eigenvalues and eigenvectors are

$$\omega_{\mathrm{n}}^{(\mathrm{k})} = \omega_{\mathrm{n}}^{(0)} + \left(\tilde{\mathbf{V}}_{\mathrm{n}}^{(0)} \cdot \mathbf{Q} \mathbf{V}_{\mathrm{n}}^{(\mathrm{k}-1)} \right) \tag{E1}$$

$$\begin{aligned} \mathbf{V}_{\mathrm{n}}^{(\mathrm{k})} = \mathbf{V}_{\mathrm{n}}^{(0)} &- \sum_{\mathrm{m_1} \neq \mathrm{n}}^{\mathrm{N}} \frac{P_{\mathrm{m_1 n}}}{\omega_{\mathrm{m_1}}^{(0)} - \omega_{\mathrm{n}}^{(\mathrm{k})}} \mathbf{V}_{\mathrm{m_1}}^{(0)} + \sum_{\mathrm{m_1} \neq \mathrm{n}}^{\mathrm{N}} \sum_{\mathrm{m_2} \neq \mathrm{n}}^{\mathrm{N}} \frac{P_{\mathrm{m_1 m_2}} P_{\mathrm{m_2 n}}}{\left[\omega_{\mathrm{m_1}}^{(0)} - \omega_{\mathrm{n}}^{(\mathrm{k})}\right]\left[\omega_{\mathrm{m_2}}^{(0)} - \omega_{\mathrm{n}}^{(\mathrm{k})}\right]} \mathbf{V}_{\mathrm{m_1}}^{(0)} \\ &+ \ldots + (-1)^{\mathrm{k}} \sum_{\mathrm{m_1} \neq \mathrm{n}}^{\mathrm{N}} \cdots \sum_{\mathrm{m_k} \neq \mathrm{n}}^{\mathrm{N}} \frac{P_{\mathrm{m_1 m_2}} P_{\mathrm{m_2 m_3}} \cdots P_{\mathrm{m_k n}}}{\left[\omega_{\mathrm{m_1}}^{(0)} - \omega_{\mathrm{n}}^{(\mathrm{k})}\right]\left[\omega_{\mathrm{m_2}}^{(0)} - \omega_{\mathrm{n}}^{(\mathrm{k})}\right] \cdots \left[\omega_{\mathrm{m_k}}^{(0)} - \omega_{\mathrm{n}}^{(\mathrm{k})}\right]} \mathbf{V}_{\mathrm{m_1}}^{(0)} \end{aligned} \tag{E2}$$

$\bar{\mathbf{V}}_{\mathrm{n}}^{(0)}$ are worked out as the solution of the adjoint of the operator $\boldsymbol{\mathcal{L}}^{(0)}$

$\boldsymbol{\mathcal{L}}^{(0)\dagger}\bar{\mathbf{V}}_{\mathrm{n}}^{(0)} = \omega_{\mathrm{n}}^{(0)}\bar{\mathbf{V}}_{\mathrm{n}}^{(0)}$.

The operator $\boldsymbol{\mathcal{L}}^{(0)}$, cast as system of first-order ODEs, is not symmetric. $\mathbf{V}_{\mathrm{n}}^{(0)}$ and $\bar{\mathbf{V}}_{\mathrm{n}}^{(0)}$ form its bi-orthogonal basis vectors, i.e.

$\bar{\mathbf{V}}_{\mathrm{m}}^{(0)} \cdot \mathbf{V}_{\mathrm{n}}^{(0)} = \delta_{mn}$.

P_{mn} is the projection of the perturbation operator $\mathbf{Q}$ on the basis space, i.e.

$P_{\mathrm{mn}} = \bar{\mathbf{V}}_{\mathrm{m}}^{(0)} \cdot \mathbf{Q}\mathbf{V}_{\mathrm{n}}^{(0)}$.